frontiers | Frontiers in Physiology

TYPE Original Research
PUBLISHED 15 May 2023
DOI 10.3389/fphys.2023.1111244

OPEN ACCESS

EDITED BY
Abhishek Chatterjee,
UMR7618 Institut d'écologie et des sciences de l'environnement de Paris (IEES), France

REVIEWED BY
André Fiala,
University of Göttingen, Germany
Claire Eschbach,
Université Paris-Saclay, France

*CORRESPONDENCE
Liria M. Masuda-Nakagawa,
lm546@cam.ac.uk

†These authors have contributed equally to the work

RECEIVED 29 November 2022
ACCEPTED 02 May 2023
PUBLISHED 15 May 2023

CITATION
Mohamed A, Malekou I, Sim T, O'Kane CJ, Maait Y, Scullion B and Masuda-Nakagawa LM (2023), Mushroom body output neurons MBON-a1/a2 define an odor intensity channel that regulates behavioral odor discrimination learning in larval *Drosophila*. *Front. Physiol.* 14:1111244. doi: 10.3389/fphys.2023.1111244

Mushroom body output neurons MBON-a1/a2 define an odor intensity channel that regulates behavioral odor discrimination learning in larval *Drosophila*

Abdulkadir Mohamed†, Iro Malekou†, Timothy Sim, Cahir J. O'Kane, Yousef Maait, Benjamin Scullion and Liria M. Masuda-Nakagawa*

Department of Genetics, University of Cambridge, Cambridge, United Kingdom

The sensitivity of animals to sensory input must be regulated to ensure that signals are detected and also discriminable. However, how circuits regulate the dynamic range of sensitivity to sensory stimuli is not well understood. A given odor is represented in the insect mushroom bodies (MBs) by sparse combinatorial coding by Kenyon cells (KCs), forming an odor quality representation. To address how intensity of sensory stimuli is processed at the level of the MB input region, the calyx, we characterized a set of novel mushroom body output neurons that respond preferentially to high odor concentrations. We show that a pair of MB calyx output neurons, MBON-a1/2, are postsynaptic in the MB calyx, where they receive extensive synaptic inputs from KC dendrites, the inhibitory feedback neuron APL, and octopaminergic sVUM1 neurons, but relatively few inputs from projection neurons. This pattern is broadly consistent in the third-instar larva as well as in the first instar connectome. MBON-a1/a2 presynaptic terminals innervate a region immediately surrounding the MB medial lobe output region in the ipsilateral and contralateral brain hemispheres. By monitoring calcium activity using jRCamP1b, we find that MBON-a1/a2 responses are odor-concentration dependent, responding only to ethyl acetate (EA) concentrations higher than a 200-fold dilution, in contrast to MB neurons which are more concentration-invariant and respond to EA dilutions as low as 10^{-4}. Optogenetic activation of the calyx-innervating sVUM1 modulatory neurons originating in the SEZ (Subesophageal zone), did not show a detectable effect on MBON-a1/a2 odor responses. Optogenetic activation of MBON-a1/a2 using CsChrimson impaired odor discrimination learning compared to controls. We propose that MBON-a1/a2 form an output channel of the calyx, summing convergent sensory and modulatory input, firing preferentially to high odor concentration, and might affect the activity of downstream MB targets.

KEYWORDS

calyx, mushroom bodies, MBONs, odor discrimination learning, intensity coding

Introduction

To respond adaptively to environmental stimuli, sensory signals defined as sensory objects (Gottfried, 2010), must be encoded in neural representations that are highly selective, to be useful for formation and retrieval of memories. The recognition of sensory objects depends on the selective pattern of activation of a few numbers of neurons at higher centers in the brain, using a combinatorial coding mechanism that is shared across different sensory modalities in insects and mammals (Perez-Orive et al., 2002; DeWeese et al., 2003; Quiroga et al., 2005; Stettler and Axel, 2009). However, the dynamic range of intensity of sensory signals can be large. For example, in vision, the dynamic range of light intensities is in the order of 10^{10}; in olfaction rats can recognize odors over a 50,000-fold range in intensity (Homma et al., 2009), and still a unique image or smell must be recognized across a large range of intensities. The control of gain in the visual pathway is found at many levels, for example, by negative feedback of horizontal cells on photoreceptors, and amacrine cells on bipolar cells, the presynaptic cells of ganglion cells. However, how different levels of intensity are encoded and integrated to generate a unique representation of a given sensory object at the higher centers of the brain is not well understood.

The olfactory system shares principles of information processing across insects and mammals, and the numerical simplicity of brains in *Drosophila*, makes it a good model to study olfactory coding. Odors are detected by olfactory sensory neurons (OSNs) in the fly antennae and maxillary palp, or dorsal organ in *Drosophila* larvae. OSNs have different affinities for their ligands, and the combinatorial pattern of their activation is represented in the antennal lobe (AL), the first olfactory center. Here, a nonlinear transformation of intensity coding takes place, weak signals are enhanced and strong signals suppressed (Bhandawat et al., 2007), a principle also found in honeybees (Sachse and Galizia, 2003). Therefore, the AL plays a role in improving signal to noise, adjusting the gain, a process that is regulated by lateral inhibition by the local inhibitory neurons (Asahina et al., 2009). Response tuning of individual OSNs in larvae studied by electrophysiological recordings, showed that individual OSNs respond to different dilutions of an odor, in a range of dilutions over 10^{-2} to 10^{-4}, and that the combined responses of OSNs allowed larvae to perceive and discriminate odors in an odor preference test (Kreher et al., 2008). Compared to projection neurons (PNs) that are broadly responsive, Kenyon cells (KCs) in the mushroom body (MB) are selective (Perez-Orive et al., 2002), suggesting a transformation in odor coding between PN input and KC processing. The anatomical organization of KCs in *Drosophila* larval MBs predicts the use of a combinatorial code for odors, generating an odor identity channel (Masuda-Nakagawa et al., 2005). KCs are quiescent and respond with one or 2 spikes to PN input, and their responses are relatively concentration-invariant compared to PNs (Stopfer et al., 2003; Ito et al., 2008). The balance between discrimination and sensitivity affects learning; higher sensitivity could improve learning, while lower sensitivity could decrease learning, while improving discrimination. In the mammalian piriform cortex, odor identity is suggested to be encoded in a subset of odor concentration-invariant piriform cortex neurons, while piriform cortex neurons can respond to a 100-fold concentration range with different odor representations (Roland et al., 2017).

To understand the neural circuitry that regulates the selectivity of sensory representations, and its regulation by odor intensity, we use the *Drosophila* larval MB calyx. MBs are centers for associative learning in the insect brain, and the calyx is the dendritic input region with a role in odor discrimination. The calyx receives stereotypic input from projection neurons (PNs) and is innervated by a feedback inhibitory neuron, the larval APL (Masuda-Nakagawa et al., 2005; 2014), and two octopaminergic neurons called sVUM1 originating in the SEZ, which can modulate behavioral odor discrimination (Wong et al., 2021). Two output neurons, named MBON-a1 and MBON-a2, arborize in the MB calyx (Eichler et al., 2017; Saumweber et al., 2018).

Odd neurons are a group of eight neurons (Slater et al., 2015) that include two neurons named MBON-a1/a2 (Eichler et al., 2017; Saumweber et al., 2018) that widely innervate the calyx of the MBs, and have been proposed to receive multiple PN inputs (Slater et al., 2015). Slater et al. (2015) showed that Odd neurons enhanced the ability to discriminate different concentrations of odors in a chemotaxis assay; however, learning was not tested. Silencing these neurons may depress appetitive learning in larvae, although this interpretation is complicated by diverse expression patterns of the *GAL4* lines used for this work (Saumweber et al., 2018).

We have shown previously that the calyx-innervating Odd neurons, MBON-a1/a2, labeled by *GAL4-OK263*, have potential synaptic contacts with both octopaminergic sVUM1 neurons, sVUMmd1 and sVUMmx1 (Wong et al., 2021), and therefore MBON-a1/a2 might be subject to modulation by OA input.

Here we characterize the connections and polarity of MBON-a1/a2 neurons in the third-instar larval calyx, and compared this using existing and new analysis of the first instar connectome (Eichler et al., 2017). We show that MBON-a1/a2 respond to odor in a concentration-dependent manner, in contrast to KCs, which are more concentration-invariant. They also affect learning performance, although not in a strongly concentration-dependent manner. MBON-a1/a2 may nonetheless represent a channel that conveys odor intensity information to the output region of the MBs, and therefore could potentially have a role in concentration-dependent modulation of MB output neurons and signals.

Materials and methods

Fly stocks

All stocks were maintained on cornmeal-yeast-agar medium at 25°C in a 12-h day/night cycle. Stocks are listed in Table 1.

Immunohistochemistry and confocal imaging

Third-instar wandering larvae (144–176 h AEL) were dissected in cold PBS, fixed in 4% Formaldehyde/PEM buffer (0.1 M PIPES; 2 mM EGTA; 1 mM $MgSO_4$; NaOH), PH 7.3, for 2 h at 4°C, washed for 3 × 10 min (or 4 × 15 min) in 0.3% Triton-X in PBS (PBT) and incubated in 10% NGS (Normal goat serum) in 0.3% PBT for 1 h at

TABLE 1 ***Drosophila*** **stocks used. Includes all genotypes used for this study, including those that do not appear in figures. The GMR designation is usually omitted for brevity in the text and figures.**

Genotype	Source	References	RRID	Use	Figure
MB242A, or: *R64FO7-p65.AD* (X); *R57C10-GAL4DBD* (III)	BDSC 68307	Aso et al. (2014)	BDSC_68307	Split GAL4 for MBON-a1/a2 neurons	1, 5, 7
GMR52E12-GAL4 (III)	BDSC 38837	Jenett et al. (2012)	BDSC_38837	MBON-a1/a2 neurons	2
NP2631-GAL4 (II)	T Awasaki, K Ito	Masuda-Nakagawa et al. (2014)	DGGR_104,266	APL neuron	2
NP225-GAL4 (II)	T Awasaki, K Ito	Masuda-Nakagawa et al. (2005)	DGGR_112,095	MBON-a1/a2	2
OK263-GAL4 (II)	CJOK, LMN	Wong et al. (2021)		MBON-a1/a2	1, 2
Mef2-GAL4 (III) (also known as MB247-GAL4)	BDSC 50742	Zars et al. (2000)	BDSC_50742	KCs	5
GMR68B12-GAL4 (III)	BDSC 39463	Jenett et al. (2012)	BDSC_39463	MBON-a1 or a2	2
Tdc2-LexA (II)	S Waddell	Burke et al. (2012)		KCs	2
MB247-LexA (III)	T Lee	Pitman et al. (2011)		KCs	2
GMR26G02-LexA (II)	BDSC 54645	Jenett et al. (2012)	BDSC_54645	APL	2
GH146-LexA (II)	A Lin	Lai et al. (2008)		PNs	2
GMR68B12-LexA (II)	BDSC 54095	Jenett et al. (2012)	BDSC_54095	MBON-a1 or a2	2
GMR57C10-LexA (II)	BDSC 52817	Jenett et al. (2012)	BDSC_52817	nSyb-LexA	
NP225-GAL4; MB247-LexA		Masuda-Nakagawa et al. (2005)		GRASP	2
GH146-LexA; GMR52E12-GAL4	This work	This work		GRASP	2, S2
GMR26G02-LexA; GMR52E12-GAL4	This work	This work		GRASP	2, S2
GH146-LexA; GMR68B12-GAL4	This work	This work		GRASP	2
GMR68B12-GAL4, MB247-LexA (III)	This work	This work		GRASP	2, S2
GH146-LexA; GMR52E12-GAL4	This work	This work		GRASP	2, S2
NP2631-GAL4; GMR68B12-LexA	This work	This work		GRASP	2
MB247-LexA; OK263-GAL4	This work	This work		GRASP	2
Tdc2-LexA; GMR52E12-GAL4	This work	This work		Live Imaging	6
UAS-Syt::GFP UAS-DenMark::mCherry (III)	BDSC 33065	Nicolaï et al. (2010)	BDSC_33065	Neuronal polarity	1
10XUAS-IVS-mCD8::RFP, 13XlexAOp2-mCD8::GFP (X)	BDSC 32229	Pfeiffer et al. (2010)	BDSC_32229	Double Reporter, to verify *GAL4 LexA* stocks	S2
UAS-CD4::spGFP1-10	K Scott	Gordon and Scott (2009)		GRASP	2
LexAop-CD4::spGFP11	K Scott	Gordon and Scott (2009)		GRASP	2
UAS-CD4::spGFP1-10; LexAop-CD4::spGFP11		Gordon and Scott (2009)		GRASP	2
UAS-CsChrimson.mVenus (III)	BDSC 55136	Klapoetke et al. (2014)	BDSC_55136	Optogenetics for behavior	1
UAS-jRCaMP1b (III)	BDSC 63793	Dana et al. (2016)	BDSC_63793	Calcium reporter	5, 6
LexAop-ChR2-XXL (II)	C Wegener (955)	Selcho et al. (2017)		Optogenetics	6
LexAop-ChR2-XXL; UAS-jRCaMP1b	This work	This work		Combined optogenetic stimulation and recording	6
Canton S	J Carlson			Behavior	7

room temperature. Brains were incubated in primary antibody in 10% NGS-0.3% PBT at 4°C for 2–3 days on a mini disk rotor (Biocraft, BC-710), washed for 3 × 15 min with 0.3% PBT and further incubated in secondary antibody in 10% NGS at 4°C for 2–3 days again on the mini disk rotor. Brains were finally washed 1 × 15 min with PBT, followed by 3 × 10 min with PBS, and left in 50%

TABLE 2 Antibodies.

Antibody	Host	Source	RRID	Dilution	Experiment or Figures
Anti-GFP	Rat, monoclonal	Nacalai 440426 (Clone GF090R)	AB_2314545	1:1000	Anatomy, GRASP, 1, 2, S2, S3
Anti-DsRed	Rabbit, polyclonal	Clontech, 632496	AB_10013483	1:1000	UAS-DenMark Brp:mCherry, 1 UAS-RFP, S2, S3
Anti-GABA	Rabbit, polyclonal	Sigma, A2052	AB_477652	1:1000	GRASP, 2
Anti-OA	Rabbit, polyclonal	MoBiTec, 1003 GE	AB_2314999	1:1000	GRASP, 2
Anti-DLG	Mouse, monoclonal	DSHB, 4F3	AB_528203	1:200	1, 2, S2, S3
Secondary Antibody	Host	Source		Dilution	
Anti-Rat Alexa 488	Goat, polyclonal	Invitrogen, A11006	AB_2534074	1:200	
Anti-Rabbit Alexa 568	Goat, polyclonal	Invitrogen, A11036	AB_10563566	1:200	
Anti-Mouse Alexa 647	Goat, polyclonal	Invitrogen, A21236	AB_141725	1:200	

TABLE 3 Other reagents.

Reagent	Source	Experiment or Figures
PBS	Sigma P4417	Anatomy, GRASP
Formaldehyde	Polysciences 18814	Anatomy, GRASP
PIPES	Sigma P1851	Anatomy, GRASP
EGTA	Sigma E3889	Anatomy, GRASP
Triton-X	Sigma T8787	Anatomy, GRASP
Normal goat serum	Vector Labs S-1000	Anatomy, GRASP
Paraffin oil	Sigma-Aldrich, 76235	Live imaging, Behavior
Pentyl Acetate	Sigma-Aldrich, 109584	Live imaging, Behavior
Ethyl Acetate	Sigma-Aldrich, 319902	Live imaging, Behavior
Ethanol	Sigma-Aldrich, 32221	Behavior
all-trans-retinal (ATR)	Sigma-Aldrich, R2500	Live imaging, Behavior
D-(−)-Fructose	Sigma-Aldrich, 47740	Behavior
Agarose	Sigma-Aldrich, A9539	Behavior

Glycerol/PBS at 4°C for at least one night prior to imaging. Primary and secondary antibodies are listed in Table 2, other reagents in Table 3. Imaging was carried out using an SP8 Confocal Microscope with a 40X NA1.3 water objective.

CATMAID

The publicly available first-instar larval connectome on CATMAID software (Saalfeld et al., 2009; Schneider-Mizell et al., 2016) on the Virtual Fly Brain site (https://l1em.catmaid.virtualflybrain.org; Licence CC-BY-SA_4.0; Court et al., 2023) was used to study neuron morphology and synaptic partners. The "Connectivity Widget" was used to find the listed presynaptic partners of MBON-a1/a2. For each presynaptic partner, the location of each of the synapses made with MBON-a1/a2 was noted by clicking on the individual synapse connector number and looking at the location shown on the 3D reconstruction of the neuron on the "3D viewer". For each of the MBON-a1/a2 neurons, the number of cyan (postsynaptic) and red (presynaptic) sites was counted three times in the calyx (due to the large number of sites) and an average was calculated; synapses in the output regions, which were fewer in number, were counted once. Graphs were generated using Microsoft Excel version 16.60 (Supplementary Table S1).

Live imaging and optogenetics

Live imaging was performed as previously described (Masuda-Nakagawa et al., 2009). Wandering stage L3 *Drosophila* were dissected and mounted for imaging under an Olympus BX50-WI microscope with a Zeiss W Plan-Apochromat 40x/1.0 DIC M27 objective and using an Andor iXon + DU-88E-CO-#BV EM-CCD camera (Andor, Belfast, United Kingdom), via a Cairn Research Optosplit II (Faversham, United Kingdom).

Wandering stage L3 larvae for combined optogenetics and imaging were dissected under dim amber (591 nm) light and the condenser light of the BX50-WI was passed through an ET632/60 M emission filter. A Cairn OptoLED LED mount (Cairn Research) on the Olympus BX50-WI BX-FLA vertical illuminator was used to illuminate the sample through the objective. The vertical illuminator aperture was minimized to a diameter of approximately twice that of the calyx (from a dorsal view) and centered within the camera's field of view. A 470 nm LED and power supply (Cairn Research, OPTOLED Light source) with an LED mount (Cairn Research, LED mount) was used alongside Polygon400 (polygon400-G) for patterned illumination. Polyscan2 software (Mightex) was used to control the illumination pattern.

Throughout the optogenetics experiment, the full camera capture region was illuminated (256 × 256 µm). A microscope slide power sensor (Thorlabs S170C) with an optical power and energy meter (Thorlabs PM400) was used to calibrate the LED and

measure the LED power at the specimen, *Tdc2-lexA* was crossed to *lexAop-jRCamP1b, lexAop-ChR2(XXL)*, and it was subsequently shown that 470 nm LED of 8.55 μW intensity applied for 500 ms was the optimal stimulus strength and duration to evoke a strong increase in calcium with minimum light exposure. A T495lpxr dichroic mirror (Chroma, VT, United States) directed the LED light onto the sample while preventing 470 nm light reflected off the sample from reaching the microscope output.

The shutter of a Yokogawa CSU22 spinning disc confocal (Yokogawa Electric Corporation) was controlled by Micro Manager (Edelstein et al., 2010), and the PC interface with the spinning disc was via the multifunction I/O card (National Instruments, PCI-6221). The camera interface was via an Andor interface card (Andor, PCI controller) and Metamorph software (Metamorph meta imaging series version 7.0) was used to control the camera settings and image acquisition. The Cairn Research (Faversham, United Kingdom) laser controller was used to deliver a 561 nm excitation laser, at 20% laser power; at this power, *LexAop-ChR2-XXL/nSyb-LexA; UAS-jRCaMP1b/MKRS* larvae showed no movement in response to the laser. The room was kept at 23°C. A Master-8-cp controller (AMPI, Jerusalem, Israel) synchronized the timing of imaging, LED illumination, and odor delivery.

Humidified odors were presented through valves controlled by the Master-8-cp controller as described (Masuda-Nakagawa et al., 2009). All crosses were performed on cornmeal-yeast-agar medium, and for optogenetics media were supplemented with 100 μM all-trans-Retinal (Sigma, R2500). Crosses were kept at 23°C in the dark wrapped in tinfoil, and when necessary handled under dim amber light (591 nm).

Combined optogenetics and activity imaging was performed by crossing *LexAop-ChR2-XXL; UAS-jRCaMP1b/TM6B* virgin females to a stock carrying *52E12-GAL4* and *Tdc2-LexA* insertions, and collecting wandering third-instar progeny. ChR2-XXL function was confirmed by crossing female parents to *nSyb-LexA/CyO:GFP* males and testing undissected, non-*CyO:GFP* larval progeny for light-induced body contraction under imaging conditions. Driver genotypes in all *GAL4* and *LexA* combination lines were tested by imaging RFP and GFP expression in the larval progeny of a cross between males of each line to virgin females of a *UAS-RFP LexAop-GFP* double reporter line (Bloomington stock 32229).

Paradigms

Concentration-dependence of MBON-a1/a2 and KC responses: a pulse of EA at different concentrations diluted in mineral oil was applied for 2 s, at 2 s after the start of image acquisition. Image acquisition was at a frame rate of 5 frames/second, for 100 ms. Image acquisition continued for a total of 12 s. Thirty-second intervals with no laser exposure were introduced between image acquisitions at different concentrations to re-establish baseline fluorescence, and the order of concentrations (increasing or decreasing) was varied between preparations. The average fluorescence of the first 10 frames of image acquisition was taken as baseline. Individual datapoints on graphs and statistical analyses represent single brain hemispheres, in most cases a single brain hemisphere per larvae, but in some cases both.

Combined optogenetics and imaging experiment: "odor only" consisted of 3 s of baseline image acquisition, followed by a 10-fold diluted EA pulse for 2 s. Frame rate and laser duration were the same as above. Image acquisition was for a total of 13 s. The average fluorescence value of the first 10 frames was taken as baseline. "Odor + Light" consisted of 2 s of baseline image acquisition, followed by a pulse of 470 nm LED for 500 ms, then an odor pulse of a 10-fold dilution of EA was applied at 3 s after the start of image acquisition for 2 s, with a total image acquisition time of 13 s. An interval of 76 s between the end of one acquisition and the start of the next was introduced to allow time for baseline recovery, according to τ_{off} for ChR2-XXL being 76 s (Dawydow et al., 2014). Frame rate and laser duration were the same as above. Pulse duration was determined by titrating time and recording increase in fluorescence in *Tdc2* neurons expressing *ChR2-XXL* and *jRCAMP1b*, near the primary processes where the signal was stronger. "Light only" was as above except that no odor pulse was applied. In control experiments using *52E12-GAL4* and *UAS-JRCaMP1b*, in the presence of a *LexAop-ChR2-XXL* construct without the *Tdc2* driver, five pulses of 470 nm LED of 50 ms were applied at 200-ms intervals for a total time of 1 s for one of two sets of experiments instead of a single 500-ms light pulse as above, but no significant differences between the two light treatments were detected in the peak responses obtained (Mann-Whitney test or t-test as appropriate), and therefore these data were merged.

Image analysis

ImageJ (Schindelin et al., 2012) was used to analyze the stacks generated by Metamorph. Areas that responded to stimuli were identified using a standard-deviation projection, and a region of interest (ROI) was drawn manually (Supplementary Figure S1), tightly around the edge of the areas with a higher standard deviation than background. The *Z*-axis profile function was then used to quantify the fluorescence changes over time which were subsequently saved as Excel files. The same ROI outline was then moved to an adjacent, non-responding region and the procedure was repeated to calculate background fluorescence over time. After subtracting background fluorescence from each frame, baseline fluorescence calculated as the average of the first 10 frames before odor delivery, were subtracted from each frame value to obtain ΔF. Normalized signal intensity ΔF/F at each time point was calculated by dividing ΔF over baseline fluorescence (Masuda-Nakagawa et al., 2014). To ensure these changes were not due to the order in which concentrations were tested (possibility for adaptation affecting the results for the later tested concentrations), randomization of the order in which the concentrations were tested was also practiced. In this experiment and subsequent experiments, data from larvae that had moved during imaging were excluded as it was impossible to tell if the fluorescence change was due to movement or an odor response. Each acquisition consisted of 60 frames of background-subtracted intensity data acquired over 12 s. To smoothen out frame-to-frame

variation, we used the overlapping moving averages of three sequential frames, leaving 58 frames of smoothed data.

Statistics

Analysis was carried out using GraphPad Prism 8 software, and statistical tests used for each experiment are shown in figure legends. Statistical significance was defined as $p < 0.05$ throughout, taking account of *post hoc* and multiple testing.

Behavioral assay

Larval culture. For testing behavioral roles of MBON-a1/a2, flies of genotype *w; 20xUAS-IVS-CsChrimson.mVenus (III)* were crossed to either the split-GAL4 line *MB242A* for MBON-a1/a2 behavior assay, or Canton S as positive control. Larvae were allowed to develop in food vials containing 100 µM all-trans-retinal, in the dark at 23°. Adults were transferred into new vials both in the morning and in the evening, and progeny collected after 136–152 h at 23°C.

Behavioral arena

Agarose Petri dishes were prepared the day before use, by using 100 ml of distilled water with 0.9% agarose (Sigma A9539). Fructose Petri dishes were prepared similarly, but containing 35% fructose (Sigma-47740). Petri dishes had perforated lids, to facilitate creation of odorant gradients within the dish, by sucking air from a benchtop fume extractor (Sentry Air Systems (SAS), SS-200-WSL) at the back of the assay platform. Odorants were diluted in paraffin oil (Sigma-Aldrich 76235) and 10 µl was added to custom-built Teflon containers with pierced lids (7 holes), on the surface of agarose plates.

Light apparatus

The light apparatus contained a BK Precision DC power pack, connected to a pulse generator, driving four sets of amber light LEDs (591 nm), Luxeon star Amber LED on Tri-Star Base, 330 lm at 350 mA (SP-03-A5). The irradiance on the platform was 0.06 µW/mm^2 on average (24 µW on a 20 × 20-mm sensor) on the 8.5-cm plate. The pulse generator was constructed as described by deVries and Clandinin (2013), by the Psychology Department workshop of the University of Cambridge. One cycle of pulses consisted of 10-ms pulses at 10Hz for 30 s, followed by 30 s without pulses. This cycle was repeated 5 times, making a conditioning step of 5 min.

Behavior conditioning

Third-instar larvae were collected from dark-reared vials using a metal sieve, and washed with tap water. This and all subsequent procedures were performed under a weak blue aquarium LED light. Larvae were washed twice by transferring through a drop of water, and then placed on the conditioning agarose plate (35% fructose). A Teflon container with 10 µl of odor A to be reinforced was placed on the left side, and another containing paraffin oil (neutral) symmetrically on the right side, at positions marked on a black background, used to facilitate visualization of the larvae. Larvae were conditioned on the fructose plate with odor A for 5 min under only the weak blue light. Larvae were then transferred to a water droplet using a brush, and again to a second water droplet to ensure no fructose traces remained, and then to an agarose plate lacking fructose, on which a Teflon container with 10 µl of odor B (non-reinforced) was placed on the left side and a container with paraffin oil (neutral) on the right side. Larvae were conditioned for 5 min under the weak blue light as above. This conditioning procedure on both plates was repeated for three cycles. For experiments using activation of OA neurons, the entire conditioning cycles were carried out under amber light from the above amber LED apparatus, in addition to the weak blue background LED.

Odor dilutions

Dilutions of ethyl acetate (EA) at 1:2000 and pentyl acetate (PA) at 1:500, and EA at 1:4000 and PA at 1:1000 diluted in mineral oil were used.

Testing

Larvae were tested by placing them on an agarose plate carrying a container with EA on one side, and a container with PA on the other. Test was under blue light for 5 min. Larvae were counted on the side of the conditioned odor, the unconditioned odor or in the neutral zone in the middle, and the performance index (PI) was calculated, using the formula:

$$PI = (N_{conditioned} - N_{unconditioned})/N_{total}$$

where:

$N_{conditioned}$: larvae on the side of the conditioned odor.

$N_{unconditioned}$: larvae on the side of the unconditioned odor.

N_{Total}: larvae on the side of conditioned odor, unconditioned odor, and middle zone.

Learning Index (LI) was calculated after both a conditioning with odor A and a reciprocal conditioning with odor B (with a different sample of larvae), using the formula:

$$LI = (PI_A - PI_B)/2$$

Statistical analysis

A two-way ANOVA using Graph Pad Prism software was used to test whether learning index was affected by odor concentration or light.

Results

MBON-a1/a2 are postsynaptic in the third-instar MB calyx

Odd neurons were defined as a group of 8 neurons, labeled by *Odd-GAL*, some of which innervate the larval calyx (Slater et al., 2015). Connectomic analyses of the first instar larva showed that two of them innervate the calyx, and these were named as MBON-a1 and MBON-a2 (Eichler et al., 2017; Saumweber et al., 2018). In the third-instar larva, two neurons with cell bodies located posteriorly to the MBs in each brain hemisphere are labeled in the split-GAL4 line *MB242A* (Aso et al., 2014) driving expression of *UAS-CsChrimson.mVenus* (Figure 1A). This is consistent with the anatomy of MBON-a1/a2 described in Supplementary figure 2 of Saumweber et al. (2018), and visualised by GFP labeling of *GAL4* line *R64F07*. This expression of *MB242A* has also

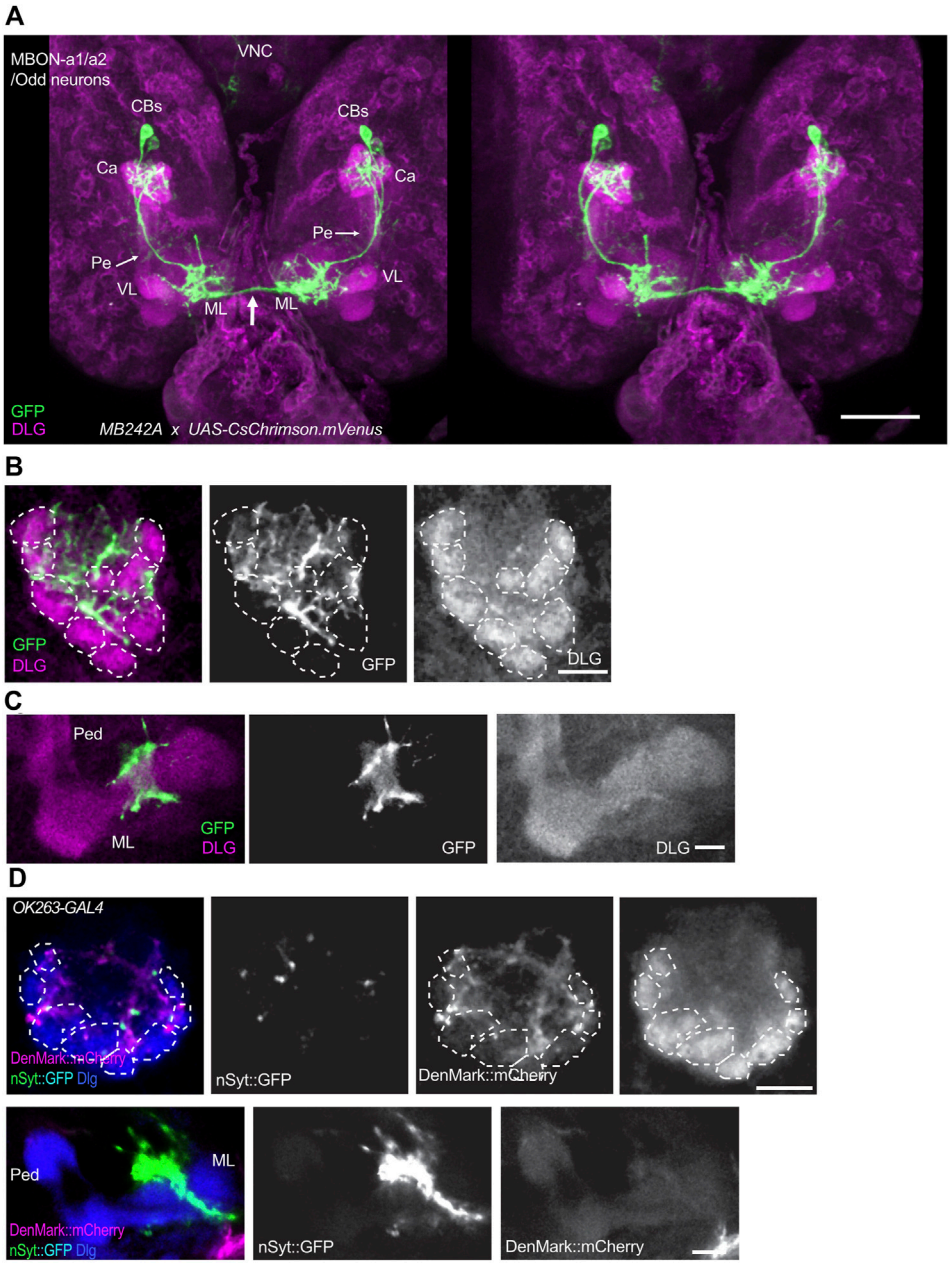

FIGURE 1
MBON-a1/a2 neurons innervate the calyx and output regions around the MB medial lobes. **(A)** A 3D stereo pair of a dorsal view of the larval central brain showing a pair of MBON-a1/a2 neurons labeled by the split-GAL4 line *MB242A* driving *UAS-CsChrimson.mVenus*. mVenus is labeled by anti-GFP, and much of the neuropil including MBs is labeled by anti-Dlg. Notice the extensive innervation by these neurons of the calyx, and the region surrounding the vertical lobe (VL) and medial lobe (ML) of the MBs. There is also some weak labeling of projections in the pedunculus (Pe, arrows). Both MBON-a1/a2 neurons also project (arrow) to the contralateral brain hemisphere. **(B)** A single section of one of the calyces shown in A, showing the dense innervation by MBON-a1/a2 throughout the calyx core and interglomerular spaces. **(C)** A single confocal section showing MBON-a1/a2 innervation of a region in the vicinity of the medial lobe of the MBs, from a ventral section of the preparation shown in **(A)**. **(D)** Projections of confocal sections of MBON-a1/a2 expressing DenMark:mCherry and Syt:GFP under the control of *OK263-GAL4*, detected by antibodies to DsRed and GFP respectively. Top row, calyx; bottom row, ML and pedunculus. Anterior is to the bottom in all panels. Glomeruli indicated by dotted lines. CBs, cell bodies; Ca, calyx; VL, vertical lobe; ML, medial lobe. Scale bars, 50 μm **(A)**, 10 μm **(B–D)**.

been described at low resolution by Hancock (2021), who also saw labeling in a single pair of subesophageal neurons that have not been characterized further. Detailed analysis of the MB242A line shows that the MBON-a1/2 primary neurites join in a tract that bifurcates anteriorly to the calyx, with one branch penetrating the calyx ventrally and branching into an extensive network throughout it, and the main process extending anteriorly to innervate a region wrapping around the ipsilateral MB medial lobe (ML), with some faint labeling also in the lower pedunculus (Figure 1A). One axon leaves here to cross the midline and innervates the equivalent regions around the contralateral ML. The innervation of the calyx is dense but localized to

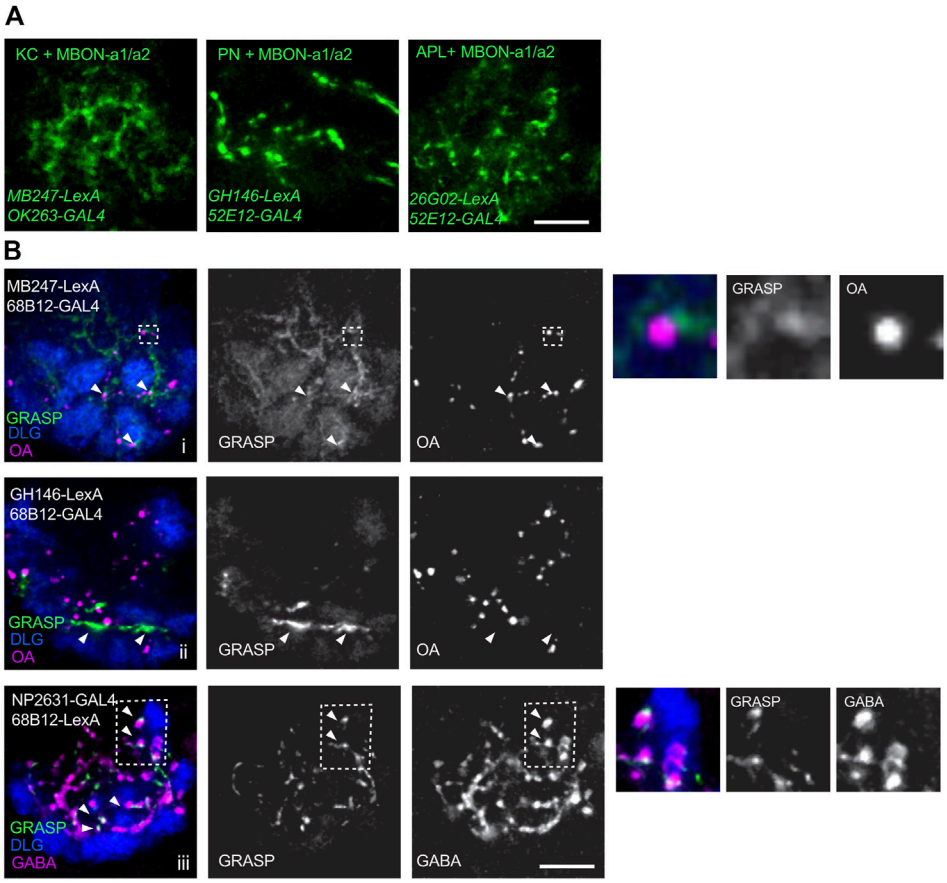

FIGURE 2
Connectivity of MBON-a1/a2 and other calyx neurons in third-instar larvae. **(A)** Live GRASP signals of MBON-a1/a2 with dendrites of KCs, axonal termini from PNs, or axonal processes of larval APL. A line carrying GRASP constructs *UAS-CD4::spGFP1-10* and *LexAop-CD4::spGFP11*, was crossed to flies containing the *GAL4* and *LexA* constructs shown. GRASP signals were detected in the third-instar wandering stage larval progeny. GRASP signal was detected as native GFP fluorescence in z-projections of a few confocal sections. All panels are right brain images, anterior to bottom. Scale bar 10 µm. **(B)** GRASP signals between one of the MBON-a1/a2 neurons and KCs, PNs, or APL visualized by immunolabeling. A line carrying GRASP constructs *UAS-CD4::spGFP1-10* and *LexAop-CD4::spGFP11* was crossed to flies containing the constructs shown. GRASP signals were detected in the third-instar wandering stage larval progeny using monoclonal rat anti-GFP. **(i)** In MBON-a1/a2-KC GRASP, arrowheads indicate GRASP signal in proximity to OA boutons. Inset inside broken line is shown enlarged to the right of the panels. **(ii)** In MBON-a1/a2-PN GRASP, GRASP signal is observed in PN axonal tracts and may not represent synaptic contacts (arrowheads). **(iii)** MBON-a1/a2-APL: arrowheads indicate co-localization of GABA and GRASP signals. Inset inside broken line is shown enlarged to the right of the panels. Calyx glomeruli are visualized using anti-Dlg. Right brain calyces are shown, anterior is to the bottom. Scale bar: 10 µm.

interglomerular spaces and the core of the calyx, avoiding the calyx glomeruli, labeled by anti-DLG, that are neuropiles with connectivity between PN boutons and KC dendritic claws (Figure 1B; Supplementary Figure S2A, B). MBON-a1/a2 arborizations show extensive overlap with the GABAergic larval APL in the calyx (Supplementary Figure S2C). They show thin processes as well as thick enlargements. GABA-containing termini are found in the vicinity of MBON-a1/a2 processes. Near the MB medial lobe, MBON-a1/a2 axons form a circle around the lobe but do not innervate it (Figure 1C). MBON-a1/a2 innervation of the calyx is mainly postsynaptic as shown by expression of the dendritic marker DenMark:mCherry (Nicolai et al., 2010), driven by *OK263-GAL4* (Wong et al., 2021), only a few puncta were seen using Syt:GFP; however, strong Syt:GFP labeling but not DenMark was observed around the region of the ML (Figure 1D), implying that these MBON-a1/a2 projections are presynaptic. Consistent with this, we also found strong localization of a second presynaptic marker, nSyb:GFP at the output regions around the ML (Supplementary Figure S2D).

Extensive contacts of MBON-a1/a2 with calyx neurons

To analyze the connectivity between MBON-a1/a2 and other calyx neurons in third-instar larvae, we used *GAL4* lines expressing in MBON-a1/a2 and *LexA* lines expressing in potential partner neurons in the calyx, for GRASP (GFP reconstitution across synaptic partners; Gordon and Scott, 2009). To verify the *GAL4* and *LexA* insertions used for GRASP, third-instar larvae carrying pairs of these insertions were used to drive the double reporter *UAS-mCD8::RFP LexAop-mCD8::GFP*, to visualize the pattern of calyx innervation (Supplementary Figure S2). *MB247-LexA*, which drives expression in KCs, shows dense labeling of the calyx, whereas MBON-a1/

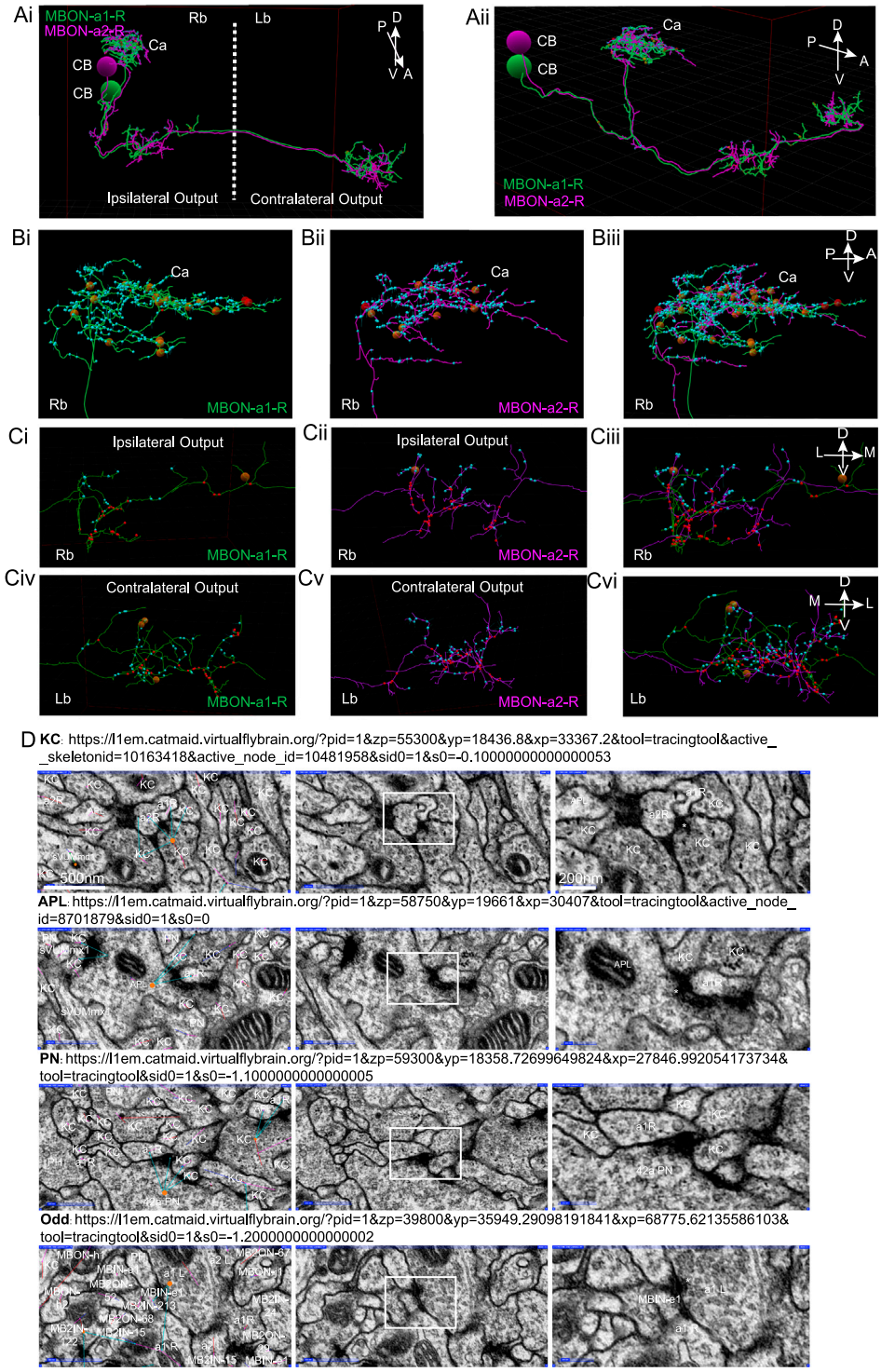

FIGURE 3
Synapses of MBON-a1/a2 visualized by CATMAID in the first instar larva. **(A)** A reconstruction using CATMAID (Eichler et al., 2017) of MBON-a1-R (annotated in CATMAID as MBE7a right) in green and MBON-a2-R (annotated as MBE7b right) in purple, showing their cell bodies (CB), projections in the calyx (Ca), and axonal regions with ipsilateral and contralateral outputs. The axes on the top right corner of the panel indicate the orientation of the neuron, where A is anterior, P is posterior, D is dorsal, V is ventral. **(Ai):** Approximately frontal view of reconstruction. **(Aii)**: A more lateral view of the same reconstruction, showing the projections of MBON-a1-R and MBON-a2-R from their posteriorly located cell bodies to the anterior and dorsal parts of the brain. **(B)** A lateral view of a reconstruction of MBON-a1-R **(Bi)** and MBON-a2-R **(Bii)** and their overlap **(Biii)** showing their projections in the right brain calyx. **(C)** Frontal view of the ipsilateral **(Ci–Ciii)** and contralateral **(Civ–Cvi)** outputs around the medial lobes of the MBs of MBON-a1-R **(Ci, Civ)** and MBON-a2-R **(Cii, Cv)** and their overlap **(Ciii, Cvi)**. In all panels, small cyan circles are MBON-a1-R and MBON-a2-R postsynaptic sites, and small red circles are presynaptic sites. The larger brown and red circles are unfinished tracing sites. The axes on the top right corner of panels **Biii, Ciii** and **Cvi** apply to each entire row. Images were generated by analysis of neuron tracing using the 3D tool of CATMAID on the publicly available first-instar larval connectome on the Virtual Fly Brain site (https://l1em.catmaid.virtualflybrain.org; Licence CC-BY-SA_4.0). Schneider-Mizell et al. (2016); Saalfeld et al. (2009). **(D)** EM
(*Continued*)

FIGURE 3 (Continued)
sections of first-instar larva MBON-a1/a2 synapses. The top three rows show presynaptic partners of MBON-a1-R (labeled as a1R) in the calyx. Each row shows examples of four common partners: a KC; an APL (labeled as MBE12 on CATMAID); and PN42a. The bottom row of panels shows MBON-a1-L (labeled as MBE7a left on CATMAID), which is presynaptic to contralateral MBON-a1-R in the output regions around the medial lobes. In each row, the left panel shows an EM section with CATMAID annotations; a connector (orange) is placed on the presynaptic neuron and the cyan arrows indicate postsynaptic partners. The middle panel shows the same EM section without the CATMAID annotations. The right panel shows a magnification of the outlined area of each middle panel, showing the characteristic vesicles and T-bar (labeled with an asterisk where present) in presynaptic boutons. The scale bars in the top row apply to all four rows.

a2 expressing *OK263-GAL4* or *52E12-GAL4* innervate the core of the calyx and interglomerular space (Supplementary Figures S2A, B, D).

The pattern of innervation of MBON-a1/a2 and the larval APL expressing *UAS-mCD8:RFP LexAop-mCD8:GFP*, in larvae carrying *26G02-LexA* and *52E12-GAL4*, shows extensive overlap of processes, and contacts around APL boutons (Supplementary Figure S2C). We used these *GAL4* and *LexA* lines to express the GRASP constructs *UAS-CD4::spGFP1-10* and *LexAop-CD4::spGFP1* in third-instar larval brains. We used a number of *GAL4* lines to label MBON-a1/a2 (Figure 2; Supplementary Figure S2) mainly due to the need for different chromosomal locations for stock construction. Extensive native GRASP GFP fluorescence was observed between MBON-a1/a2 on the one hand, and KCs, PNs, and APL on the other (Figure 2A).

We also confirmed the occurrence and localization of GRASP signals in the third-instar wandering stage larvae by antibody labeling. Brains were immunolabeled to visualize glomeruli by anti-DLG (Parnas et al., 2001), GFP by rat monoclonal anti-GFP, and subsets of synaptic sites were visualized by anti-octopamine (OA) for MBON-a1/a2-KC or MBON-a1/a2-PN connectivity, and anti-GABA for MBON-a1/a2-APL connectivity. KC-MBON-a1/a2 GRASP showed a diffuse pattern through much of the calyx, with some GRASP signals localized in the vicinity of OA boutons, suggesting a synaptic localization for some of the signals, consistent with the MBON-a1/a2 contacts with sVUM1 neurons seen previously using GRASP (Wong et al., 2021). These were in the calyx core, or interglomerular space (Figure 2Bi, arrows and inset). MBON-a1/a2-PN GRASP showed a strong signal that we interpret as axonal tracts because of their length along the borders with glomeruli. It is hard to determine whether some synaptic contacts were present between PN axonal tracts and MBON-a1/a2 dendrites (Figure 2Bii). MBON-a1/a2-APL GRASP showed the characteristic GRASP puncta, and their synaptic localization is shown by co-localization with GABA. Many GRASP signals are also observed in the core of the calyx and in the interglomerular space (Figure 2Biii). Control crosses lacking single *GAL4* or *LexA* constructs, that are both required for expression of both GRASP components, showed no localized anti-GFP signal (Supplementary Figure S3).

Pattern of innervation of MBON-a1/a2 in the first instar larva

In the first instar larva connectome, a pair of calyx-innervating mushroom body output neurons have been annotated in the CATMAID tool as MBON-a1-R, and MBON-a2-R in the larval right brain hemisphere, and another pair MBON-a1-L and MBON-a2-L in the left brain hemisphere (Eichler et al., 2017). While these authors identified partner neurons and counted synaptic contacts with them, (Supplementary Tables 1, 2 of Eichler et al., 2017), we wanted greater clarity on the spatial distribution of the inputs of calyx-innervating neurons in the calyx. We therefore manually counted MBON-a1/a2 synaptic sites in the calyx (Figure 3A), and found these to be predominantly postsynaptic (Figure 3Bi-iii, Supplementary Table S1). MBON-a1/a2 processes in the output regions around the ipsilateral and contralateral MB medial lobes contained both postsynaptic as well as presynaptic sites (Figure 3C; Supplementary Figure S4; Supplementary Table S2), this contrasts with the polarity seen in our third-instar larval data (Figure 1D), where synapses are predominantly presynaptic in the output region. There was extensive regional overlap in the pattern of innervation of the calyx by both MBON-a1 and MBON-a2 (Figure 3Bi-iii), as well as in the output region in the ipsilateral (Figure 3Ci-iii) and contralateral brain (Figure 3Civ-vi).

Figure 3D shows representative synapses onto MBON-a1/a2 marked in CATMAID: (1) presynaptic terminals of KCs and APL in the calyx, with vesicles and T-bars synapsing on MBON-a1/a2, (Figure 3D top 2 rows); (2) a presynaptic terminal of PN42a containing vesicles, in the calyx on MBON-a1-R (Figure 3D, 2nd row from bottom); (3) a presynaptic terminal of MBON-a1-L onto MBON-a1-R in the output region, suggesting the presence of synapses between MBON-a1/a2 there (Figure 3D, bottom row). In the calyx only a few synapses were from MBON-a1/a2 onto KCs, PN13a, and sVUM1s, and no synapses were presynaptic to APL.

To define the number of inputs for each of the MBON-a1/a2 neurons from their input neurons in the calyx, we manually identified the presynaptic and postsynaptic sites for each of the MBON-a1/a2 neurons on the 3D skeleton in CATMAID, according to regional localization, e.g., calyx or non-calyx regions (Supplementary Data File S1, S2). In the right calyx we counted some 338 input sites for MBON-a1-R and 368 for MBON-a2-R, a total of 706 input sites in the right calyx, and in the left calyx, 262 for MBON-a1-L and 429 for MBON-a2-L. Our numbers are slightly lower than those of Eichler et al. (2017); our analysis (Supplementary Data File S2) indicates that this is largely due to them counting input sites outside the calyx, in the axonal and presynaptic compartments of MBON-a1/a2, as dendritic inputs.

We found approximately 90% of inputs in the calyx from KCs (Figure 4): 303 synapses for MBON-a1-R, 333 for MBON-a2-R, 244 for MBON-a1-L, and 389 for MBON-a2-L. These numbers are again lower than the numbers of KC inputs into MBON dendrites reported by Eichler et al. (2017); again this is largely due to some KC inputs into MBON-a1/a2 around the latter's output region, including some onto the contralateral projections in their analysis (Supplementary Data File S2; Connectivity matrix Table 1 of Eichler et al., 2017). The large fraction of calyx inputs from KCs is consistent with the widespread GRASP signal between KCs and one of the MBON-a neurons (Figure 2). Of the

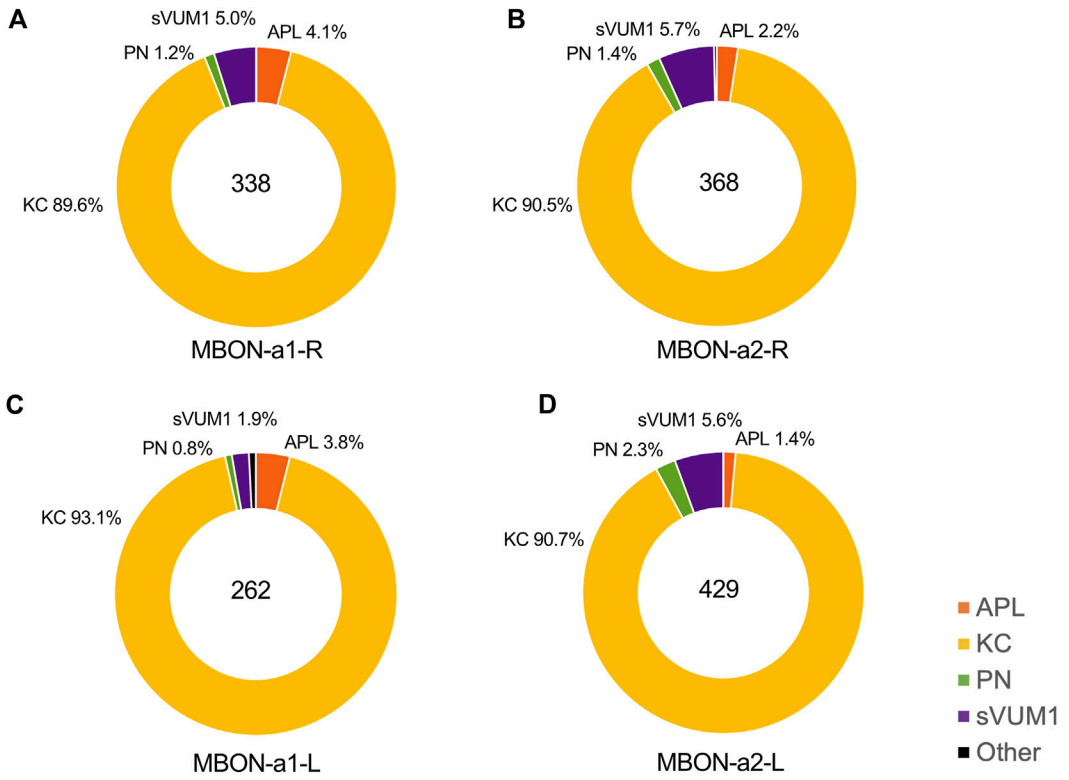

FIGURE 4
The types of neurons presynaptic to MBON-a1/a2 in the calyx. This figure shows the proportion of KCs, APL, PN, sVUM1 neurons and other neurons that provide input to MBON-a1/a2 in the calyx. These were calculated from CATMAID data by dividing the number of presynaptic inputs to MBON-a1/a2 from each neuron type by the total number of annotated inputs of each MBON-a1/a2 neuron in the calyx (See Materials and Methods). APLs are shown in orange, KCs in yellow, PNs in green, sVUM1s in purple and other types of neurons in black. Individual panels show the types of calyx presynaptic partners of **(A)** MBON-a1-R, **(B)** MBON-a2-R, **(C)** MBON-a1-L and **(D)** MBON-a2-L.

72 mature KCs on the right brain in the first instar connectome (Supplementary Table 1 of Eichler et al., 2017), 67 have inputs into at least one of MBON-a1/a2, and in most cases into both; and of 73 mature KCs on the left brain, all but two do; very few immature KCs show inputs into the MBON-a1/a2 neurons. This near-universal connectivity from KCs onto MBON-a1 and a2 suggests that both these MBON neurons could potentially sample and integrate signals from KC activity from across the calyx.

The proportions of presynaptic partner inputs onto the other MBON-a1/a2 neurons were similar to those on MBON-a1-R (Figure 4). There was no preference for synapses with particular types of KC; KC39, KC54, and KC77 have three to four dendrites that are spread out, while dendrites of KC34, KC25, and KC49 KC22 were localized to a subregion of the calyx for the right brain. Some KCs provide input to both MBON-a1/a2 neurons in the right brain.

PN, sVUM1s, APL inputs to MBON-a1/a2 in the calyx

The second main inputs to MBON-a1/a2 in the calyx are from the two sVUM1 neurons (OAN-a1/a2), with 17 inputs (5% of total) onto MBON-a1-R. Our numbers (Supplementary Data Files S1, S2) are in agreement with those in Supplementary Adjacency Matrix 2 of Eschbach et al. (2020), and all the sVUM1 to MBON-a1/a2 connections that we observe are in the calyx.

After this, APL has 14 inputs (4% of the total) to MBON-a1-R, which is significant considering that there is only a single larval APL in each side of the brain (Figure 4). APL in the right brain has 14 and 8 presynaptic sites on MBON-a1-R and MBON-a2-R, respectively, while APL in the left brain has 10 and 6 presynaptic sites and MBON-a1-L and MBON-a2-L, respectively. We found APL to MBON-a1/a2 connections only in the calyx and not around the lobes, where APL also arborizes (Supplementary Data Files S1, S2).

The number of inputs onto MBON-a1/a2 neurons from PNs was only around 1% for MBON-a1-R, 4 synapses out of 349. These numbers are surprisingly low, considering that there are over 40 PN inputs in the calyx (of which 21 are olfactory), and raises the question of whether these connections are functionally significant. Also arguing against significant PN-MBON-a1/a2 connectivity, the EM sections of PN-MBON-a1/a2 synapses did not meet most of the synapse criteria, e.g., a PN42a synapse showed no T-bar, postsynaptic density or synaptic cleft (Figure 3D, second row from bottom), supporting the doubts on the roles of PN-MBON-a1/a2 contacts in the calyx.

Mix of pre and post synapses in the output regions of MBON-a1/a2

In the calyx, we counted only 6 presynaptic sites in MBON-a1/a2 in the right calyx and none in the left calyx; for MBON-a1-R, one is presynaptic to sVUM1 neurons OAN-a1 and OAN-a2, a second one to 2 KCs, a third one to a KC and OAN-a1, and the fourth one to PN13a and a KC. MBON-a2-R is presynaptic to 2 KCs, and in a divergent synapse to an unidentified "place holder neuron" and 2 KCs. MBON-a1/a2 had no presynapses onto APL. Therefore, MBON-a1/a2 arborizations are mainly postsynaptic in the calyx (Supplementary Table S1), and their sparse presynaptic connections may be of limited functional significance.

On the other hand, the output region of the MBON-a1/a2 around the MB medial lobe contained a mix of postsynaptic and presynaptic sites, segregated in axonal branches that were compartmentalized into either mainly presynaptic or postsynaptic sites (Figure 3Ci–Cvi). The number of presynaptic sites for MBON-a1-R in the right brain was 35, and 33 for MBON-a2-R, a total of 68; the equivalent numbers of postsynaptic sites were 20 for MBON-a1-R and 36 for MBON-a2-R, a total of 56. Similar numbers were counted in the contralateral left brain (Supplementary Table S2), where MBON-a1 and MBON-a2 had similar numbers of synapses (Supplementary Table S3). Therefore, the output regions of MBON-a1 and MBON-a2 contain comparable numbers of presynaptic and postsynaptic regions, in the ipsilateral and contralateral output regions. Interestingly, MBON-a1/a2 target many MBONs and MB inputs in this area (Supplementary Figure S5).

Some reciprocal synapses between MBON-a1 and MBON-a2 were also found in the output region, e.g., Figure 3D. All four MBON-a1/-a2 neurons have synaptic connections among themselves, numbering between 1 and 8, and no differences were detected between ipsilateral and contralateral partners (Supplementary Table S3). There were no annotated synapses between MBON-a1/MBON-a2 neurons in the calyx. Only 11 presynaptic sites onto KCs were annotated in the lobes (e.g., Supplementary Figure S6), indicating that MBON-a1/a2 do not provide significant output to KCs around the medial lobes.

Consistent with the faint labeling of MBON-a1/a2 projections in the third-instar pedunculus (Figure 1A), we also found some inputs into these neurons in this region in the first-instar connectome – mostly 1-2 inputs from individual KCs, with each of the different MBON-a1/a2 neurons receiving inputs from 3–13 KCs. The small fraction of the 72–73 KCs with such inputs, together with the low numbers of inputs, does not suggest the pedunculus as a site for responses by the MBON-a1/a2 neurons to KC inputs generally. However, there are exceptions: the two "thermosensory KCs" (Eichler et al., 2017) made between 2 and 13 inputs into three of the four MBON-a1/a2 neurons, potentially suggesting a regulation of MBON-a1/a2 activity by temperature (Supplementary Data File S2).

Odor concentration dependence of MBON-a1/a2 neuron responses

Despite the lack of strong GRASP or anatomical evidence for PN-MBON-a1/a2 contacts, Odd neurons have been implicated in concentration-dependent behavioral responses to odors (Slater et al., 2015). We therefore analyzed the concentration-dependence of MBON-a1/a2 responses to odors, by expressing the genetically encoded calcium indicator *jRCaMP1b* (Dana et al., 2016) in MBON-a1/a2 using the split-GAL4 line *MB242A* (Figure 1), and recorded calcium responses to different concentrations of ethylacetate (EA). For comparison, we also assayed odor responses using *jRCaMP1b* expressed in KCs, known to have more concentration-invariant responses (Stopfer et al., 2003).

Odor-evoked activity was observed throughout MBON-a1/a2, including in the calyx and output regions around the ML. In the calyx, activity was predominantly localized to regions around glomeruli (Figure 5A, left panel); the latter interpretation is consistent with the interglomerular localization of MBON-a1/a2 processes (Figure 1B). Some activity was also observed in the non-glomerular calyx core, and the dendritic shaft that leaves the calyx (Figure 5A, arrow). The odor-evoked response pattern of MBON-a1/a2 in the calyx is similar to the activity of KCs in response to EA, where a few glomeruli are activated by EA (Figure 5A, right panel), as expected from our previous observation that odors are represented in a spatially localized pattern in the calyx (Masuda-Nakagawa et al., 2009). Since *MB247-GAL4* is a strong driver that labels most KCs, of which there are about 2100 at larval wandering stage (Technau and Heisenberg, 1982), and KCs show a dense pattern of innervation of the calyx in glomerular and non-glomerular regions, a strong baseline fluorescence was observed.

The MBON-a1/a2 odor response began at the onset of the odor pulse, except for the lowest dilution at 1/200 where the small increase started only at the end of the odor pulse (Figure 5B). The time course of KC responses showed a similar temporal pattern at the onset of the odor pulse, but the ΔF/F values were lower (Figure 5B). This could potentially be an effect of the high baseline fluorescence observed in the calyx using the *MB247-GAL4* driver.

MBON-a1/a2 responded to high concentrations of odors, e.g., 1/10 dilution of EA, but not to 1/200 and very weakly to 1/100 dilutions of EA (Figure 5B). The peak ΔF/F gradually decreased with increasing odor dilution, with a 1/100 dilution of EA giving a mean response around 21% of that of a 1/10 dilution, and a 1/200 dilution only 10%, and not statistically different from zero ($p = 0.194$, two-tailed t-test). The number of preps without an odor response increased from 0% at 1/10 dilution, to 1-2 at 1/50 and 1/100 dilutions, and at 1/200 dilution only 2 preps out of 7 showed a detectable odor response. These findings suggest that MBON-a1/a2 responses have a narrow dynamic range, but are strongly concentration-dependent (Figure 5C), with a slope that is significantly different to zero in a linear regression analysis.

In contrast, the odor-evoked responses of KCs were less concentration-dependent. For all odor dilutions, KC responses closely followed odor onset. At all EA dilutions except for 1/10000, a clear odor-evoked response was observed, and 25% of preparations were non-responsive at 1/10000. KC responses were less concentration-dependent than those of MBON-a1/a2, showing similar peak ΔF/F at EA dilutions of 1/10, 1/50, 1/100, 1/1000, and only a shallow slope in the regression analysis (Figure 5C).

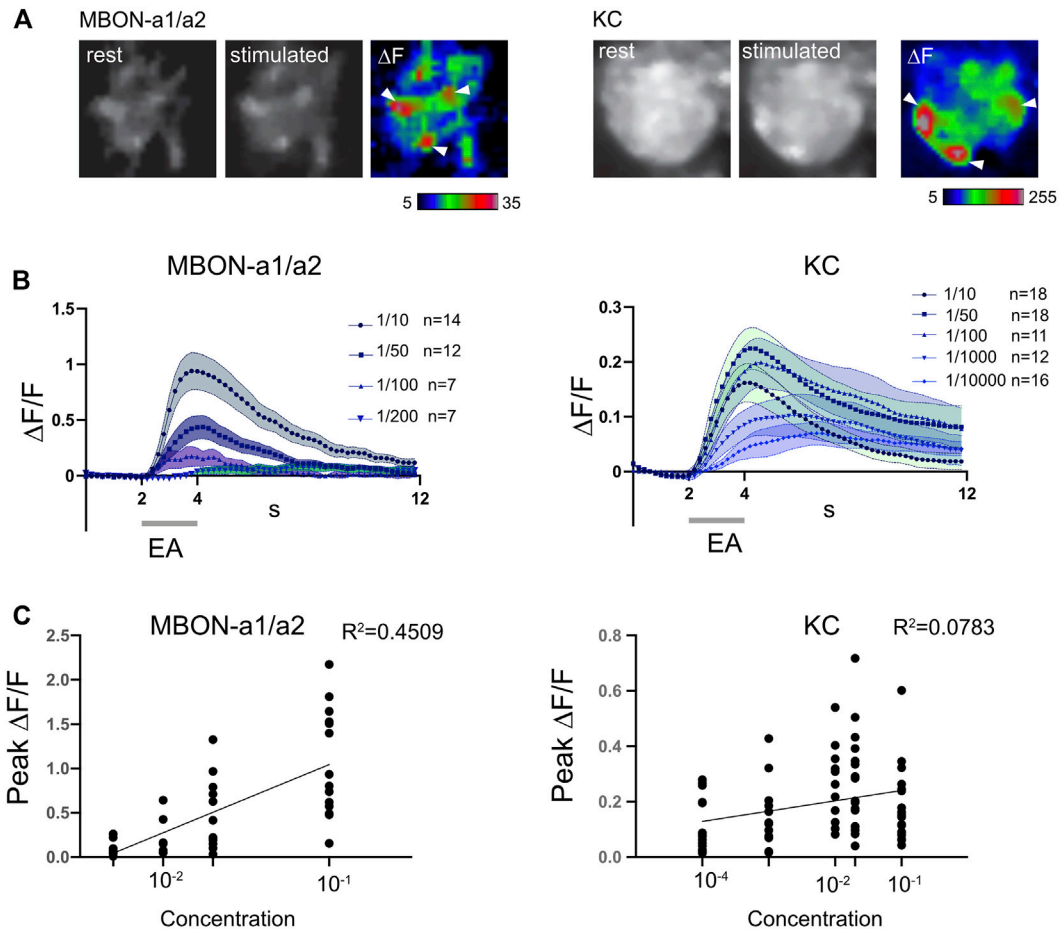

FIGURE 5
MBON-a1/a2 responses to changes in concentration of ethyl acetate are more graded than KC responses. **(A)** Odor-evoked activity in MBON-a1/a2 expressing *UAS-jRCamP1b* using *MB242A* (left panels) and in KCs expressing *MB247-GAL4* (right panels) in response to a 2-s pulse of ethylacetate (EA) diluted 10-fold in mineral oil. Resting and peak fluorescence are shown in greyscale, and ΔF in pseudocolor. White arrowheads show areas of elevated response levels corresponding to glomeruli in the KC panels, and which may represent areas adjacent to specific glomeruli in the MBON-a1/a2 panels. **(B)** Time course of odor-evoked responses to different concentrations of ethylacetate (EA) in MBON-a1/a2 or KCs. A 2-s odor pulse is indicated by a grey bar. Graphs show mean ± SEM. A three-point moving average was used to smoothen responses. **(C)** Graphs of peak ΔF/F against log(concentration of ethyl acetate), with each individual data point shown. Each line represents the calculated linear regression for MBON-a1/a2: Y = 0.7696X + 1.814, R^2 = 0.4509, slope significantly different from 0 (two-tailed $p < 0.0001$****) with the Pearson test. Linear regression for KCs: Y = 0.03727X + 0.2779, R^2 = 0.07827, slope significantly different from 0 (two-tailed $p = 0.0151$*) with the Pearson test.

Optogenetic stimulation of OA neurons does not have a detectable effect on odor-evoked responses in MBON-a1/a2

The calyx of the larval MBs is densely innervated by the terminals of octopaminergic neurons. We have previously shown that MBON-a1/a2 labeled by *OK263-GAL4* have potential synaptic contacts with *Tdc2*-expressing octopaminergic neurons innervating the calyx (Wong et al., 2021). Since octopamine is structurally and functionally similar to noradrenaline, and is a positive modulator of circuit activity (Roeder, 2005; Strother et al., 2018), we tested whether activity of *Tdc2*-OA neurons could potentially enhance odor responses in MBON-a1/a2. We measured MBON-a1/a2 odor-evoked responses using *52E12-GAL4* and *UAS-JRCaMP1b*, in the presence of a *LexAop-ChR2-XXL* construct and the OA driver line *Tdc2-LexA*, and in control larvae lacking either *LexAop-ChR2-XXL* or *Tdc2-LexA*. We measured responses in individual calyces, and the output region of MBON-a1/a2 to (sequentially) (i) an odor pulse ("odor-only"); (ii) an odor pulse delivered immediately after the end of a blue light pulse ("light + odor"). In one set of experiments, procedures (i) and (ii) were followed by (iii) a pulse of blue light to activate ChR2-XXL if expressed ("light-only").

In larvae of the experimental genotype, odor-evoked responses in MBON-a1/a2 in the calyx, were localized to a few high-activity regions that resemble interglomerular spaces or regions bordering glomeruli, consistent with the dense innervation of MBON-a1/a2 ramifying throughout the non-glomerular regions of the calyx (Figure 6A). In the output region in the vicinity of the ML (Figure 1C), an odor-evoked response was observed all along the axonal processes of MBON-a1/a2 (Figure 6A, right panels). The time course of the odor-evoked response (ΔF/F) showed an increase in response after the

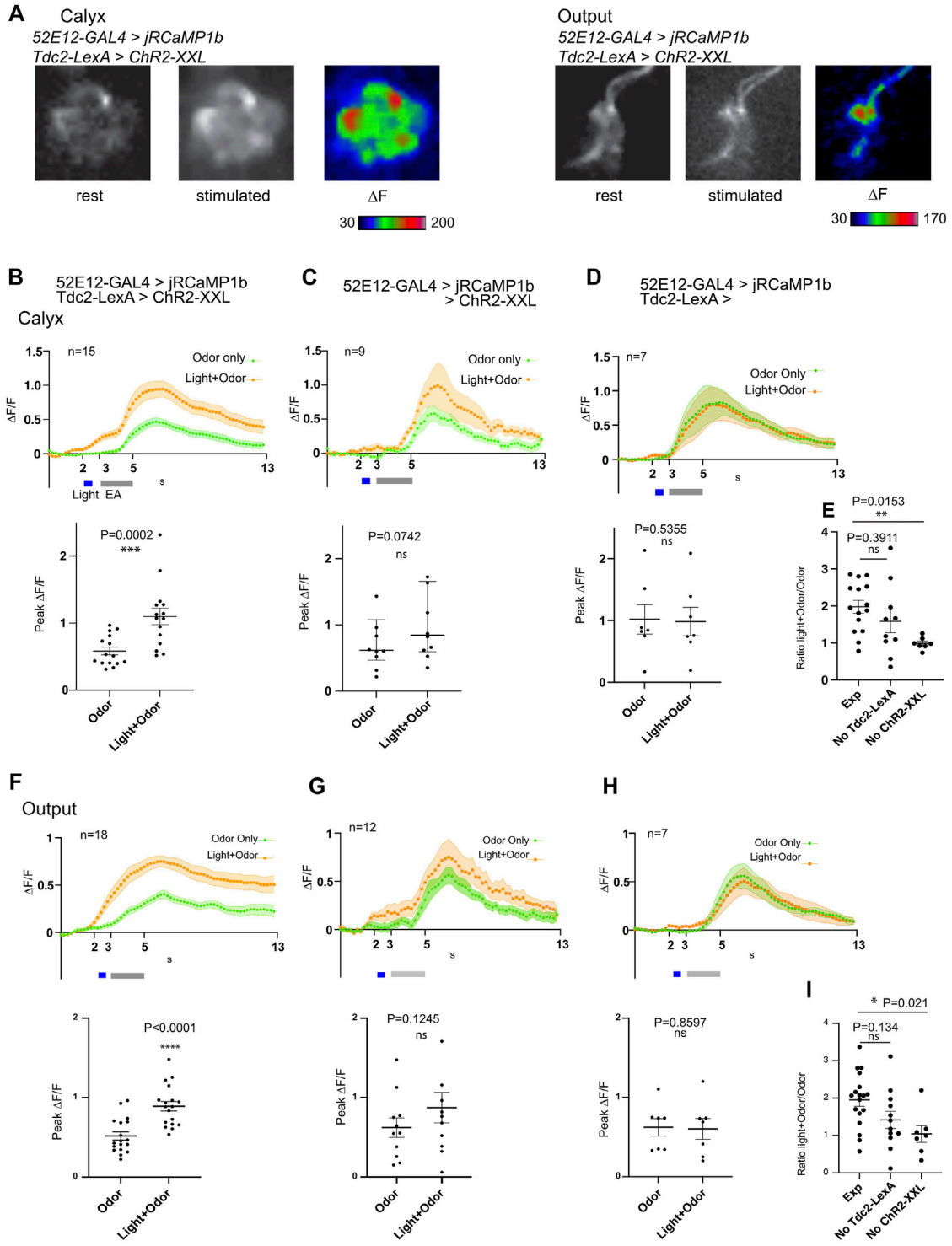

FIGURE 6
Activation of Tdc2-expressing neurons has only an additive effect on odor-evoked activity of MBON-a1/a2 in the calyx and axonal region. **(A)** Odor-evoked activity in MBON-a1/a2 expressing *UAS-jRCamP1b* under the control of *52E12-GAL4*, and carrying *Tdc2-LexA* driving *LeAop-ChR2-XXL*, to a 2s pulse of ethylacetate (EA) diluted 10-fold in mineral oil, after previous 561-nm light exposure to activate ChR2-XXL. Responses in the calyx (left panels) or the axonal output area around the ML as shown in Figure 1C (right panels) are shown. Projections of confocal images in grayscale show fluorescence at rest before odor stimulation, and after stimulation, and ΔF shown in color. **(B)** Time course of odor responses of MBON-a1/a2 to a 2s pulse of EA in the same brains either before or after light stimulation to activate ChR2-XXL in *Tdc2-LexA*-expressing neurons, in the calyx. Genotype is as in **(A)**. The upper graph shows a time course with mean ± SEM of ΔF/F, and a three-point moving average was used to smoothen responses. The grey bar shows the EA pulse, and the light pulse (for Light + Odor) is shown in blue. The scatter graph shows peak odor-evoked responses, without light stimulation (Odor) or following optogenetic stimulation (Light + Odor). Data from two sets of crosses were merged; a t-test showed no significant difference between the peak ΔF/F values from the 2 crosses. **(C)** Time courses of MBON-a1/a2 odor responses in larvae of the same genotype as A, but lacking *Tdc2-LexA*, stimulated by odor only or odor-evoked response after previous light pulse as in **(B)**. Normality for the peak ΔF/F responses could not be proven, therefore the time
(*Continued*)

FIGURE 6 (Continued)
course shows median values, and the scatter graph shows peak ΔF/F responses with median and interquartile range. Data from two sets of crosses were merged; a Mann-Whitney test showed no significant difference between the peak ΔF/F values from the 2 crosses. **(D)** Time courses of MBON-a1/a2 responses, and peak ΔF/F responses, from larvae of the same genotype as A but lacking the *LexAop-ChR2-XXL* reporter, stimulated by odor only or odor-evoked response after previous light pulses as in **(B)**. **(E)** Comparisons of the ratio of peak ΔF/F in Light + Odor conditions to that in Odor conditions in the calyx, between larvae of the same genotype as A and B, and controls lacking either *Tdc2-LexA* (as in C) or *LexAop-Chr2-XXL* (as in D). Comparisons by an ordinary one-way ANOVA test followed by Tukey multiple comparison tests are shown. **(F–I)** Responses and comparisons as in panels **(B–E)** respectively, but measured in the MBON-a1/a2 axonal output region around the ML. Peak ΔF/F values in G met a normality test and therefore data are plotted as mean ± SEM, and compared using a t-test. In all quantitation panels, data were tested for normality using a Kolmogorov-Smirnov test. In Panels **(B–D)** and **(F–H)**, time courses of normally distributed data are shown as mean ± SEM. For non-normally distributed data **(C)**, only median is shown. Normally distributed peak ΔF/F responses are presented in scatter graphs as larval datapoints, mean ± SEM, and compared using a two-tailed paired t-test. Non-normally distributed peak ΔF/F responses are presented in scatter plots as larval datapoints, median ± interquartile range, and compared using a two-tailed Wilcoxon test. Occasional outlier datapoints are omitted from the scatter graphs, but included in all statistical analyses. For **(E, I)**, normality within each data set was confirmed using a Kolmogorov-Smirnov test. The graph shows individual larval datapoints, mean ± SEM.

onset of the odor pulse for "Odor only", whereas Light + Odor showed an increase starting with the light pulse, suggesting that there is an odor-independent effect of light activation of ChR2-XXL on the activity of MBON-a1/a2 (Figure 6B). Comparisons between "Odor only" odor-evoked peak ΔF/F with and without prior light pulses showed that the difference is significant (Figure 6B, bottom panel).

To directly compare the effect of specific activation of ChR2-XXL in Tdc2-neurons with responses in controls, we compared the ratio of "Light + Odor" to "Odor only" peak responses, between larvae of the experimental genotype, and larvae lacking the expression of either *Tdc2-LexA* (hence potentially expressing *ChR2-XXL* non-specifically), or larvae lacking the *ChR2-XXL* (Figure 6E). In agreement with the measurements in Figures 6B–D, this ratio was higher in the experimental genotype compared to both controls, but only the effect of lacking ChR2-XXL was significant; the effect of lacking *Tdc2-LexA* was not significant (Figure 6E). The results suggests that there is an effect of light on MBON-a1/a2 responses that may be caused by non-specific expression of ChR2-XXL. In the output region around the MB medial lobes, where we are measuring axonal or presynaptic responses (Figure 1D; Figure 6A, right panels), our findings (Figures 6F–I) were consistent with the those in the calyx, again suggesting an effect of light on ChR2-XXL activation that is non-specific to *Tdc2* neuron activity. Comparisons using total responses integrated over the time after response onset also give similar overall conclusions (Supplementary Figure S7).

The theoretical sum of Odor-only response and the Light-only response closely matched that of the odor-evoked response with prior light pulses, and showed no significant difference in their peak (ΔF/F) responses, suggesting that the effect of a prior light pulse on the odor response of the experimental genotype can be accounted for by an additive effect of light and odor (Supplementary Figure S8Ai-Aiii), and is not due to regulation of MBON-a1/a2 responses by *Tdc2-LexA* neurons. We reached a similar conclusion for MBON-a1/a2 responses in the output region, albeit with a lower response to light-only stimulation (Supplementary Figure S8Bi-iii). Taken together, we therefore find no evidence for an effect of sVUM1 neuron activity on odor-evoked MBON-a1/a2 activity under the conditions tested here.

Optogenetic activation of MBON-a1/a2 neurons impairs behavioral odor discrimination learning

MBON-a1/a2 responds only to higher concentrations of odors (Figure 5). We therefore tested the hypothesis that MBON-a1/a2 neurons affect discrimination learning in an odor concentration-dependent manner, by optogenetic activation of MBON-a1/a2 using the long-wavelength-absorbing channelrhodopsin, CsChrimson (Klapoetke et al., 2014) driven by the split *GAL4* line *MB242A)*. As controls we used the progeny of the *CantonS* line crossed to the reporter *UAS-CsChrimson*, and of the *CantonS* line crossed to *MB242A*. We measured learning scores in a fructose-reward odor-choice learning assay (Aceves-Piña and Quinn, 1979; Scherer et al., 2003) after conditioning with amber light (to activate CsChrimson if expressed) or blue light as control, at two different concentrations of the conditioned stimuli EA and pentyl acetate (PA): a higher concentration with dilutions of EA2000:PA500 and a lower concentration with dilutions of EA4000:PA1000. A lower concentration of EA8000:PA 2000, gave only low learning scores of under 0.09 in blue light in the experimental cross (Supplementary Figure S9), and so was not analyzed further.

Activation of MBON-a1/a2 neurons in amber light during conditioning led to a lowered learning score compared to blue light at both odorant concentrations tested (Figure 7). A 2-way ANOVA test on this genotype showed a significant effect of amber light ($p = 0.0193$), and no significant effect of concentration ($p > 0.4$). While conditioning under amber light appeared to have a larger effect at the higher odorant concentration than at the lower one, ANOVA showed no significant interaction between light and concentration ($p > 0.6$), suggesting that the effect of light (and CsChrimson activation in MBON-a1/a2) was statistically indistinguishable across both concentrations. A similar analysis of the two control crosses showed no effect of amber light, showing that the depression of learning scores by amber light was dependent on the presence of both the *MB242A* genotype and the *UAS-CsChrimson* genotype, and arguing against any amber-light-sensitivity of learning in either the *MB242A*, *UAS-CsChrimson*, or *CantonS* genetic backgrounds. We therefore conclude that activation of MBON-a1/a2 impairs olfactory discrimination reward learning in larvae, but that there is not a statistically detectable dependence of this effect on odor concentration.

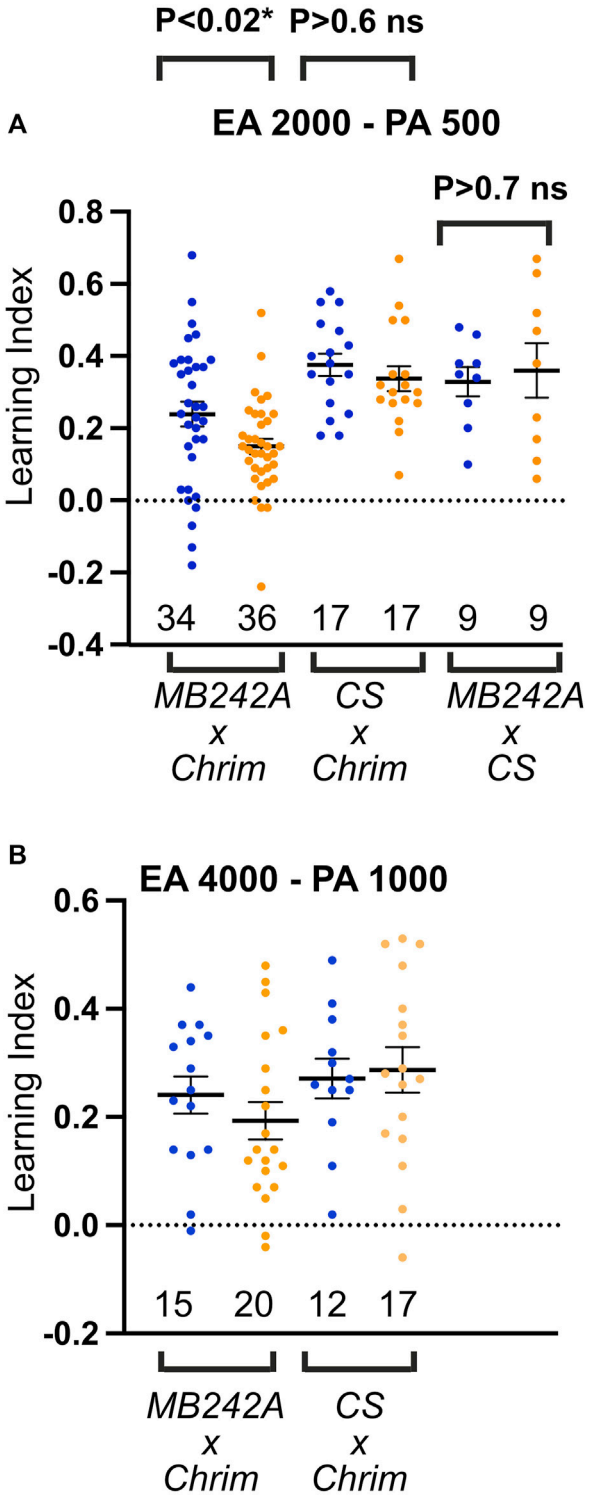

FIGURE 7
Activation of MBON-a1/a2 impairs odor discrimination learning. **(A)** Odor discrimination learning using EA at 1/2000 and PA at 1/500 dilution. Blue dots and amber dots indicate conditioning under blue light, or under amber light, which activates CsChrimson. Genotypes were the progeny of *UAS-CsChrimson* (*Chrim*) crossed to either the split-GAL4 line *MB242A* or to *CantonS* controls (*CS*), and *MB242A* crossed to *CantonS* controls. **(B)** Similar to A, using EA at 1/4000, and PA at 1/1000 dilution, and with only *UAS-CsChrimson* x *CantonS* control cross. Two-way ANOVA (light and concentration) shows a significant effect of amber light on learning across both

(*Continued*)

FIGURE 7 (Continued)
concentrations for MBON-a1/a2 activation (p = 0.0193), but no significant effect on learning scores in *CSxCrim* controls lacking *MB242A* (p = 0.69). Interaction between light and concentration was not significant in ANOVA (p = 0.64), showing that the effect of MBON-a1/a2 activation on learning was not concentration-dependent within the range of concentrations tested. No significant effect of light is seen when *MB242A* is crossed to CantonS (p = 0.72, unpaired t-test).

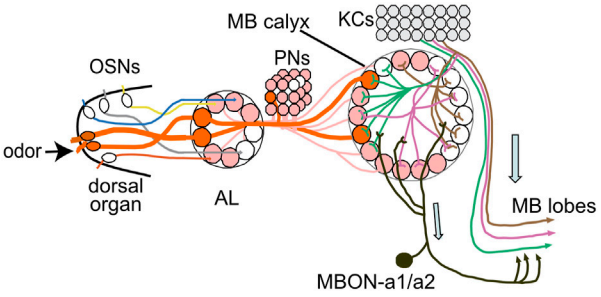

FIGURE 8
MBONa1/a2 in the wider MB circuitry. The calyx receives stereotypic input from PNs that originate mainly from single olfactory sensory neurons (OSNs) that each innervate a single AL glomerulus. KCs innervate up to 6 calyx glomeruli in a random pattern, and output in the MB lobes. MBON-a1/a2 receives inputs in the calyx, predominantly from KC dendrites, and ouput into a region surrounding the MB medial lobes. Only the ipsilateral side is drawn. Modified after Masuda-Nakagawa et al. (2014).

Discussion

MBON-a1/a2 show major contacts with KCs, APL, and sVUM1s but not PNs

The larval calyx is organized in about 34 glomeruli, sites of PN cholinergic terminal boutons synapsing with KC dendrites that are visualized by anti-DLG as the shape of a bouquet of round structures around a central core (Masuda-Nakagawa et al., 2005). MBON-a1/a2 arborize in the core of the calyx and interglomerular space, with processes abutting glomeruli but clearly avoiding their interior, suggesting that synapses onto MBON-a1/a2 occur at non-glomerular space, suggesting that they might not receive direct PN input.

Contrary to our expectations based on Slater et al. (2015), who showed GRASP signals between PNs and Odd neurons in the calyx, GRASP signals were rare or atypical between PNs and the MBON-a1 or MBON-a2 labeled *by 68B12-GAL4*. Long axonal tracts bordering the inner surface of a few glomeruli were observed labeled with GFP. The possibility exists that MBON-a1/a2 would make synapses with PNs in the core of the calyx, where PN axons are also traversing, however, GRASP signal between MBON-a1/a2 and PNs were not observed in the core of the calyx. Our evidence favors the view that PNs do not provide direct input onto MBON-a1/a2, suggesting that olfactory input is not delivered directly onto MBON-a1/a2 by the olfactory PNs.

We have shown previously that MBON-a1/a2 labeled by *OK263-GAL4* have many contacts with OA neurons at interglomerular sites (Wong et al., 2021; Figure 3D). Here we have shown that KCs also have contact sites with either MBON-a1 or MBON-a2 labeled by *68B12-GAL4* in regions neighboring glomeruli. GRASP signals between KCs and MBON-a1/a2 resemble a mesh rather than the typical dot-like signals. This might be caused by the density of KC processes in the core of the calyx and limited space between glomeruli making it easier for MBON-a1/a2 processes to come in close proximity to KC processes. Nevertheless, typical GRASP signals with high GFP intensity were seen near OA labeling, suggesting proximity to synapses between KCs and sVUM1 neurons (Figure 2B), a feature observed in previous EM analysis, showing divergent synapses of sVUM1 neurons onto MBON-a1/a2, APL and KCs (Wong et al., 2021; Figure 5E bottom three panels). KC dendrites are known to have presynaptic sites at a distance from the dendritic region containing the synapses between PNs and KCs (Christiansen et al., 2011), therefore KC contacts in the calyx core or interglomerular space could be KC presynaptic sites onto MBON-a1/a2.

Contacts between the larval APL and the single MBON-a1/a2 neuron labeled by *68B12-GAL4* formed characteristic dot-like GRASP signals, that overlapped with GABA often at one end of a large GABAergic APL bouton (Figure 2Biii). Not all GABA termini showed GRASP signals, and GRASP signals were in the calyx core and interglomerular space. Since APL is presynaptic in the calyx (Wong et al., 2021), this suggests that APL synapses onto MBON-a1/a2.

MBON-a1/a2 processes have a clear polarity (Figure 1D): in the calyx processes are mainly postsynaptic, labeled by the postsynaptic marker DenMark:mCherry, and only a few puncta labeled by Syt:GFP or n-Syb:GFP (Supplementary Figure S2D), whereas the output region surrounding the medial lobe is presynaptic and labeled by Syt:GFP and nSyb:GFP, suggesting that MBON-a1/a2 receive inputs predominantly at the calyx. This suggests that APL, sVUM1s, and even KCs are likely presynaptic to MBON-a1/a2 in the calyx, suggesting a role for MBON-a1/a2 as integrators of multiple inputs, rather that relay neurons of olfactory input. Therefore, MBON-a1/a2 neurons could be monitoring the overall activity levels in the calyx, by summing KC postsynaptic activity, in a non-odor specific manner. This would make them more concerned with activity levels than odor quality.

Comparison with the first instar connectome

The first-instar (6-h) larva connectome provides a comprehensive map of synaptic connections (Eichler et al., 2017). However, neurons can be immature at this stage, and therefore we compared the annotated connections with those in the more mature third-instar larvae. MBON-a1/a2 in the connectome shows a similar morphology to the third instar; 2 neurons have been annotated with similar and spatially overlapping projections to the calyx, ipsilateral medial lobe and contralateral medial lobe. MBON-a1/a2 processes in the first-instar calyx were postsynaptic: in the right brain, only 6 synapses were presynaptic compared to more than 600 postsynaptic sites, in agreement with our observations in third-instar larvae.

We have previously shown that at the EM level, sVUM1 neurons have divergent synapses onto MBON-a1/a2, KCs and APL; and that these synapses are surrounded by many KC processes (Wong et al., 2021; Figure 5E bottom three panels). Here we found that synapses of KCs on MBON-a1/a2 are also divergent, synapsing onto MBON-a1, MBON-a2, and KCs (Figure 3D, top panel); APL also shows divergent synapses onto MBON-a1 and a KC. Therefore, in the calyx synapses between the different types of calyx neurons, KCs, APL, sVUM1s, and MBON-a1/a2 appear to be co-localized. This is consistent with our GRASP analysis between KCs and MBON-a1/a2, where GRASP signal co-localizes with OA labeling in the calyx, suggesting the presence of synaptically rich regions localized to regions that neighbor glomeruli or in the core of the calyx.

Our CATMAID analysis shows that only a few olfactory PNs synapse onto MBON-a1/a2. Since there are at least 21 olfactory PNs, it is unlikely that PNs are a major input into MBON-a1/a2. This is consistent with our GRASP results in which GRASP signals between PNs and MBON-a1/a2 labeled tracts with no distinct punctate localization, suggesting that the signal on tracts may not be synaptic contacts as interpreted by Slater et al., 2015 (Figure 3A).

Consistent with Eichler et al. (2017, extended data file 6), we found that KCs are the major input to MBON-a1/a2 in the calyx. We counted fewer input synapses from KCs on each of the MBON-a1/a2 in the calyx, compared to the numbers reported in the Eichler et al. paper, and suggest that synapses outside the calyx might have been counted as "synapses on dendrites of MBON-a1/a2" in the Eichler et al. paper; by including synapses outside the calyx to our own calyx synapse numbers we can approximate the synapse numbers reported in the Eichler paper. Likewise this would explain our lower count for the total number of synapse inputs from all neurons into the calyx.

KCs form more than 700 synapses onto MBON-a1/a2 in the right brain calyx, which are 90% of total MBON-a1/a2 calyx inputs, and considering that there are 72–73 mature KCs in each brain hemisphere, and most of them have contacts with MBON-a1/a2, while immature KCs have only a few contacts, consistent with the view that all KCs could input into MBON-a1/a2. Only around 20% of KCs input into sVUM1 and APL also have inputs into MBON-a1/a2, suggesting that MBON-a1/a2 can be activated by KCs, but also integrate calyx inhibitory and modulatory input.

A difference from the third-instar larvae was found in the output region of first-instar MBON-a1/a2, where synapses were a mix of pre- and post -synaptic sites without a defined polarity: 68 presynaptic sites and 56 postsynaptic sites in the right brain. However, there was a regional segregation of these synapses, with branches that were exclusively presynaptic or postsynaptic. This is in contrast to the third-instar output region which appears exclusively presynaptic using presynaptic and dendritic markers (Figure 1D). This might be due to a developmental issue, if the postsynaptic projections in the medial lobe contain immature synapses that are subsequently removed or pruned. Immature synapses are common at this stage; for example, for KCs, nearly 65% are immature, defined

by lack of dendrites, or tiny dendrites and processes with endings typical of growth cones (Eichler et al., 2017). The output region had synapses between MBON-a1/a2 in CATMAID; however, presynaptic vesicles were ambiguous and there were only a small number of synapses (Supplementary Table S3), questioning whether these were true synapses. However, this observation raises the possibility that MBON-a1/a2 may provide bidirectional input to each other.

Concentration dependence of MBON-a1/a2

Our anatomical studies show that MBON-a1/a2 neurons ramify extensively throughout the calyx core and interglomerular space and receive few direct PN inputs, casting doubt on whether they might be activated by odor input. However, specific expression of jRCAMP1b in MBON-a1/a2 using the split line *MB242A* showed odor-evoked response in the postsynaptic dendrites in the calyx at localized regions (Figures 5, 6). Moreover, the response was concentration-dependent, showing graded responses to increasing concentrations of odor. The dynamic range was narrow, lying between a 10-fold and 200-fold dilutions, and the latter concentration gave only a negligible response. In sharp contrast, KCs responded to odors at a dilution as low as 10^{-4}. Also in adult flies, KCs respond to odorant dilutions of 10^{-5} to 10^{-2} (Wang et al., 2004). Therefore, MBON-a1/a2 neurons have a relatively high threshold of activation. While ΔF/F measurements do not reflect absolute levels of activity, we had no trouble in detecting MBON-a1/2 dendrites prior to stimulation (Figure 6A) and would have been able to detect ΔF responses at lower odor concentrations. Their extensive ramification in the calyx predicts a high capacitance that could rise the threshold of firing, compared to KCs, which innervate only one to six glomeruli in the larva (Masuda-Nakagawa et al., 2005; Eichler et al., 2017). This is the first time that the specific concentration-dependence of MBON-a1/a2 is reported; Slater et al. (2015) analyzed concentration-dependence for the apple cider vinegar, ACV, in *Odd-GAL4*-expressing cell bodies, that they reported to label 8 neurons including 3 innervating the calyx, only within a relatively high concentration range of 10-fold–20-fold dilution. The concentration dependence of MBON-a1/a2 reported here, in light of their anatomical organization that shows no regional arborization of dendrites in the calyx, suggests that they have a role in odor intensity coding, as opposed to KCs that work in a combinatorial mechanism that allows odor discrimination and encoding of many odors.

CATMAID and GRASP analysis in third-instar larvae are consistent with MBON-a1/a2 receiving their major input from KCs, sVUM1s, and APL neurons innervating the calyx. This implies that the source of olfactory input onto MBON-a1/a2 might be an indirect activation of MBON-a1/a2 mediated by other calyx neurons; for example, KC dendrites, and APL terminals in the calyx (Masuda-Nakagawa et al., 2014) are activated by odors. KCs are known to possess presynapses at the dendrites in the calyx (Christiansen et al., 2011) and would be the most obvious candidate to activate MBON-a1/a2 dendrites. The odor-evoked response by KCs in the calyx, showed activation of a few glomeruli, consistent with one odor activating a few olfactory receptors that act in a combinatorial manner (Hallem et al., 2004). In flies it has also been shown that the EA-evoked odor response in KCs localizes to particular calycal areas (Wang et al., 2004). The odor-evoked response of MBON-a1/a2 in the calyx also showed preferential localized activation, as opposed to whole activation of the dendritic processes in the calyx, similar to the pattern of localized glomerular activation observed in the calyx by the odor-evoked activation of KCs, suggesting that MBON-a1/a2 dendritic processes in the vicinity of KC processes activated in glomeruli by PN input, might receive input from KCs. The picture that emerges is that MBON-a1/a2 are postsynaptic to KCs, generating an output channel that encodes the intensity of olfactory input indirectly (Figure 8).

State dependent signals and MBON-a1/a2

Octopaminergic neurons are positive neuromodulators of circuit function, for example, in the motion vision system in the fly, they provide input to motion detection neurons and are involved in their temporal tuning, by increasing the excitability of medulla input neurons (Strother et al., 2018). We have previously shown that activation of sVUM1s OA neurons innervating the calyx, impair the behavioral discrimination of sensory stimuli (Wong et al., 2021), suggesting a role of calyx-innervating OA neurons in modulating calyx circuit activity. To test whether sVUM1 neurons in the calyx would modulate the excitability of MBON-a1/a2, we activated Tdc2 neurons, by optogenetic stimulation of ChR2-XXL. Localized odor-evoked responses were observed in both the calyx and output region of MBON-a1/a2 upon prior optogenetic activation of sVUM1 neurons, similar to an odor response in the specific split line (Figure 5A). The time course of odor plus light response in the calyx showed an earlier rise immediately after the light pulse and was also longer lasting than the odor only response which return to baseline after 13 s, showing that light alone has an effect on MBON-a1/a2 activity. On the other hand in the output region, the odor response did not return to baseline after 13 s, and the light plus odor response still remained high after 13 s. The difference between the response in the calyx and the output response could be mediated by the larval APL, a feedback neuron, that would shut down the response in the calyx, since MBON-a1/a2 receive significant input from APL in the calyx, also shown by GRASP signals between MBON-a1/a2 and APL.

When comparing the theoretical sum of the light only response and odor only response to the experimental odor-evoked response with prior light stimulation, there was no enhancement of the odor-evoked response in MBON-a1/a2 in the calyx nor the output region, but only an additive effect of light stimulation. It is interesting to note that the light only response of MBON-a1/a2 in the calyx shows an increase in response, while the light only response in the output region showed no increase by light alone, suggesting that the effect of light is specific to the activation of ChR2-XXL upstream of the MBON-a1/a2 in the calyx. Our controls without driver Tdc-GAL4 showed no statistically significant difference between odor-evoked response with or without prior light stimulation, suggesting that at least some effect could originate in Tdc2 activation. Therefore, activation of sVUM1 neurons did not have a significant effect on the enhancement of the odor response in MBON-a1/a2.

Behavioral role of MBON-a1/a2

Mishra et al. (2013) have shown that learnability in *Drosophila larvae* is dependent on the odor intensity at training, i.e., when the

concentration at training matches the concentration of testing in an associative learning paradigm, larvae perform more efficient learning compared to lower or higher concentrations of the conditioning odor during testing. Therefore, the learning circuits in the MBs, must have mechanisms to adjust the intensity of odor signal for optimal learning.

The neural basis of associative learning resides at the output synapses between KCs on MBONs that innervate the lobes in a compartment specific manner (Owald et al., 2015). Therefore, these are synaptic sites where learning-related plasticity could be induced. In our CATMAID analysis we observed that MBON-a1/a2 are presynaptic to many MBONs, as well as modulatory MBINs (Supplementary Figure S5), suggesting that they can be involved in the regulation of MB outputs. Could MBON-a1/a2 signals regulate KC-MBON synapses to achieve homeostatic control? Homeostatic matching has been reported in flies at the OSN-PN synapse: here strong odor stimuli would cause depression of PN responses to so that PN responses would be transient, a mechanism that would promote perceptual adaptation, and also discriminability of weak signals (Kazama and Wilson, 2008). In this scenario MBON-a1/a2, signaling a stimulus intensity largely over its threshold, could depress synapses in the KC output region around the lobes, and modify plasticity and hence learning. Such a model could potentially explain how MBON-a1/a2 activation could impair learning scores – not by affecting association itself which is thought to occur at KC/DAN synapses, but by regulating the strength of the behavioral responses to association, via regulation of other MBONs.

In odor discrimination, subsets of KCs at the core of the MBs, named "on" and "off" cells, have been proposed to function antagonistically to encode increase or decrease of odor intensity, respectively, in an odor discrimination test (Vrontou et al., 2021). They proposed that MBONs innervating the core region of the MBs lobes would be integrating both on and off signals, and the synapses between these both types of KCs and MBONs represent the plasticity site involved in learning; However, on off KCs have yet to be identified. In the larva, there is only one type of gamma KC, and although we can not rule out such "on" and "off" KCs, MBON-a1/a2 could potentially be a high-intensity channel and contribute to mediating intensity coding in reinforcement learning.

The only evidence for a role of MBON-a1/a2 in odor discrimination comes from studies in Odd neurons by Slater et al. (2015). They found that silencing Odd neurons impairs chemotaxis, while exciting them enhances chemotaxis, and concluded that Odd neurons increase behavioral sensitivity to odor concentrations. Larvae in which Odd neurons were activated could sense 4-fold differences in odor concentration (although at a very high concentration of acid vinegar at 1:4, two to three orders of magnitude higher than the dilutions that we used for learning). Also, when the output of MBON-a1/a2 is blocked by expressing *UAS-shi*^{ts} in a simplified reward association task, there was an impairment in preference index, the authors have not commented on this, but it might support a role for MBONs in regulating the formation of odor associations. (Supplementary Figure 5 of Saumweber et al., 2018).

Perspectives

Behavior depends on the precise recognition of sensory cues, however, signals in the environment range not only in its quality but also across different intensity levels. Then, how can an odor object become associated with a given context, even across different intensities?

Here, we found a pair of neurons, MBON-a1/a2, that may sense intensity odor signals indirectly via KCs, and that could potentially transmit these signals to output neuropils surrounding the output region of the MBs. Moreover, the prediction is that MBON-a1/a2 receive the same regulation as KCs, by receiving inhibitory input via APL, and neuromodulation from octopaminergic sVUM1 neurons. Therefore, MBON-a1/a2 would carry not only odor intensity input, but this would be subject to inhibition and modulation, representing a dynamic read-out of the activity state of the calyx upon stimulation of its inputs. Furthermore, since MBON-a1/a2 respond preferentially to high concentrations of odor, it could potentially be channeling an odor concentration-dependent pathway that would be integrated with the quality channel of KCs, at the level of the MBONs around the MB lobes. MBON-a1/a2 form synapses with many MBONs (Supplementary Figure S5), and elucidation of downstream partners has the potential to unravel the neural mechanism of the regulation of learning at the MB output synapses. The calyx of the MBs shows remarkable similarity in function and network organization to the piriform cortex of mammals. It is interesting to note that in the mammalian piriform cortex, different separate subsets of piriform cortex neurons have been proposed to carry concentration-invariant odor quality information and concentration-dependent intensity information (Roland et al., 2017). Therefore, the *Drosophila* larval calyx, with a small number of neurons, access to a connectome, and straightforward genetic tools, has the potential to unravel novel universal mechanisms of the regulation of learning.

Data availability statement

The original contributions presented in the study are included in the article/Supplementary Material, further inquiries can be directed to the corresponding author.

Author contributions

LMM-N: Conceived the work. LMM-N, CJO′K, TS, and AM: Experimental design. LMM-N, AM, TS, YM, and BS: Performed experiments. LMM-N, IM, AM, TS, and CJO′K: Data analysis. LMM-N: Paper drafting and writing. All authors: Editing and Reviewing. All authors contributed to the article and approved the submitted version.

Funding

The work was partially funded by BBSRC BB/N007948/1 to LMM-N and CJO'K; YM and BS were funded by summer bursaries from Magdalene College, University of Cambridge.

Acknowledgments

We thank M. Morgan for help in building the optogenetic behavioural apparatus, and Alex McLachlan for technical support. We thank Scott Waddell, Tzumin Lee, Andrew Lin, Kristin Scott and especially the Bloomington *Drosophila* Stock

Center for fly stocks, and the Developmental Studies Hybridoma Bank for antibodies. YM and BS were supported by summer research bursaries from Magdalene College of the University of Cambridge. The work was partly supported by BBSRC grant BB/N007948/1 to LMM-N and CJO′K. We thank the Department of Genetics, University of Cambridge, for infrastructural support for LMM-N.

Conflict of interest

The authors declare that the research was conducted in the absence of any commercial or financial relationships that could be construed as a potential conflict of interest.

Publisher's note

Supplementary material

The Supplementary Material for this article can be found online at: https://www.frontiersin.org/articles/10.3389/fphys.2023.1111244/full#supplementary-material

References

Aceves-Piña, E. O., and Quinn, W. G. (1979). Learning in normal and mutant *Drosophila* larvae. *Science* 206, 93–96. doi:10.1126/science.206.4414.93

Asahina, K., Louis, M., Piccinotti, S., and Vosshall, L. B. (2009). A circuit supporting concentration-invariant odor perception in *Drosophila*. *J. Biol.* 8, 9. doi:10.1186/jbiol108

Aso, Y., Sitaraman, D., Ichinose, T., Kaun, K. R., Vogt, K., Belliart-Guérin, G., et al. (2014). Mushroom body output neurons encode valence and guide memory-based action selection in *Drosophila*. *eLife* 3, e04580. doi:10.7554/eLife.04580

Bhandawat, V., Olsen, S. R., Gouwens, N. W., Schlief, M. L., and Wilson, R. I. (2007). Sensory processing in the *Drosophila* antennal lobe increases reliability and separability of ensemble odor representations. *Nat. Neurosci.* 10, 1474–1482. doi:10.1038/nn1976

Burke, C. J., Huetteroth, W., Owald, D., Perisse, E., Krashes, M. J., Das, G., et al. (2012). Layered reward signaling through octopamine and dopamine in *Drosophila*. *Nature* 492, 433–437. doi:10.1038/nature11614

Christiansen, F., Zube, C., Andlauer, T. F. M., Wichmann, C., Fouquet, W., Owald, D., et al. (2011). Presynapses in Kenyon cell dendrites in the mushroom body calyx of *Drosophila*. *J. Neurosci.* 31, 9696–9707. doi:10.1523/JNEUROSCI.6542-10.2011

Court, R., Costa, M., Pilgrim, C., Millburn, G., Holmes, A., McLachlan, A., et al. (2023). Virtual fly brain—an interactive atlas of the *Drosophila* nervous system. *Front. Physiol.* 14, 1076533. doi:10.3389/fphys.2023.1076533

Dana, H., Mohar, B., Sun, Y., Narayan, S., Gordus, A., Hasseman, J. P., et al. (2016). Sensitive red protein calcium indicators for imaging neural activity. *eLife* 5, e12727. doi:10.7554/eLife.12727

Dawydow, A., Gueta, R., Ljaschenko, D., Ullrich, S., Hermann, M., Ehmann, N., et al. (2014). Channelrhodopsin-2-XXL, a powerful optogenetic tool for low-light applications. *Proc. Natl. Acad. Sci. U. S. A.* 111, 13972–13977. doi:10.1073/pnas.1408269111

DeWeese, M. R., Wehr, M., and Zador, A. M. (2003). Binary spiking in auditory cortex. *J. Neurosci.* 23, 7940–7949. doi:10.1523/JNEUROSCI.23-21-07940.2003

Edelstein, A., Amodaj, N., Hoover, K., Vale, R., and Stuurman, N. (2010). Computer control of microscopes using μManager. *Curr. Protoc. Mol. Biol.* 92, Unit14.20. doi:10.1002/0471142727.mb1420s92

Eichler, K., Li, F., Litwin-Kumar, A., Park, Y., Andrade, I., Schneider-Mizell, C. M., et al. (2017). The complete connectome of a learning and memory centre in an insect brain. *Nature* 548, 175–182. doi:10.1038/nature23455

Eschbach, C., Fushiki, A., Winding, M., Afonso, B., Andrade, I. V., Cocanougher, B. T., et al. (2021). Circuits for integrating learned and innate valences in the insect brain. *eLife* 10, e62567. doi:10.7554/eLife.62567

Eschbach, C., Fushiki, A., Winding, M., Schneider-Mizell, C. M., Shao, M., Arruda, R., et al. (2020). Recurrent architecture for adaptive regulation of learning in the insect brain. *Nat. Neurosci.* 23, 544–555. doi:10.1038/s41593-020-0607-9

Gordon, M. D., and Scott, K. (2009). Motor control in a *Drosophila* taste circuit. *Neuron* 61, 373–384. doi:10.1016/j.neuron.2008.12.033

Gottfried, J. A. (2010). Central mechanisms of odour object perception. *Nat. Rev. Neurosci.* 11, 628–641. doi:10.1038/nrn2883

Hallem, E. A., Ho, M. G., and Carlson, J. R. (2004). The molecular basis of odor coding in the *Drosophila* antenna. *Cell* 117, 965–979. doi:10.1016/j.cell.2004.05.012

Hancock, C. E. (2021). Neural principles underlying learning and memory in *Drosophila melanogaster*. *Univ. Goettingen*. doi:10.53846/goediss-8498

Homma, R., Cohen, L. B., Kosmidis, E. K., and Youngentob, S. L. (2009). Perceptual stability during dramatic changes in olfactory bulb activation maps and dramatic declines in activation amplitudes. *Eur. J. Neurosci.* 29, 1027–1034. doi:10.1111/j.1460-9568.2009.06644.x

Ito, I., Ong, R. C., Raman, B., and Stopfer, M. (2008). Sparse odor representation and olfactory learning. *Nat. Neurosci.* 11, 1177–1184. doi:10.1038/nn.2192

Jenett, A., Rubin, G. M., Ngo, T.-T. B., Shepherd, D., Murphy, C., Dionne, H., et al. (2012). A *GAL4*-Driver line resource for *Drosophila* neurobiology. *Cell Rep.* 2, 991–1001. doi:10.1016/j.celrep.2012.09.011

Kazama, H., and Wilson, R. I. (2008). Homeostatic matching and nonlinear amplification at identified central synapses. *Neuron* 58, 401–413. doi:10.1016/j.neuron.2008.02.030

Klapoetke, N. C., Murata, Y., Kim, S. S., Pulver, S. R., Birdsey-Benson, A., Cho, Y. K., et al. (2014). Independent optical excitation of distinct neural populations. *Nat. Methods* 11, 338–346. doi:10.1038/nmeth.2836

Kreher, S. A., Mathew, D., Kim, J., and Carlson, J. R. (2008). Translation of sensory input into behavioral output via an olfactory system. *Neuron* 59, 110–124. doi:10.1016/j.neuron.2008.06.010

Lai, S.-L., Awasaki, T., Ito, K., and Lee, T. (2008). Clonal analysis of *Drosophila* antennal lobe neurons: Diverse neuronal architectures in the lateral neuroblast lineage. *Development* 135, 2883–2893. doi:10.1242/dev.024380

Masuda-Nakagawa, L., Gendre, N., O'Kane, C. J., and Stocker, R. F. (2009). Localized olfactory representation in mushroom bodies of *Drosophila* larvae. *Proc. Natl. Acad. Sci.* 106, 10314–10319. doi:10.1073/pnas.0900178106

Masuda-Nakagawa, L. M., Ito, K., Awasaki, T., and O'Kane, C. J. (2014). A single GABAergic neuron mediates feedback of odor-evoked signals in the mushroom body of larval Drosophila. *Drosoph. Front. Neural Circuits* 8, 35. doi:10.3389/fncir.2014.00035

Masuda-Nakagawa, L. M., Tanaka, N. K., and O'Kane, C. J. (2005). Stereotypic and random patterns of connectivity in the larval mushroom body calyx of *Drosophila*. *Proc. Natl. Acad. Sci. U. S. A.* 102, 19027–19032. doi:10.1073/pnas.0509643102

Mishra, D., Chen, Y., Yarali, A., Oguz, T., and Gerber, B. (2013). Olfactory memories are intensity specific in larval *Drosophila*. *J. Exp. Biol.* 216, 1552–1560. doi:10.1242/jeb.082222

Nicolaï, L. J. J., Ramaekers, A., Raemaekers, T., Drozdzecki, A., Mauss, A. S., Yan, J., et al. (2010). Genetically encoded dendritic marker sheds light on neuronal connectivity in *Drosophila*. *Proc. Natl. Acad. Sci. U. S. A.* 107, 20553–20558. doi:10.1073/pnas.1010198107

Owald, D., Felsenberg, J., Talbot, C. B., Das, G., Perisse, E., Huetteroth, W., et al. (2015). Activity of defined mushroom body output neurons underlies learned olfactory behavior in *Drosophila*. *Neuron* 86, 417–427. doi:10.1016/j.neuron.2015.03.025

Parnas, D., Haghighi, A. P., Fetter, R. D., Kim, S. W., and Goodman, C. S. (2001). Regulation of postsynaptic structure and protein localization by the Rho-type guanine nucleotide exchange factor dPix. *Neuron* 32, 415–424. doi:10.1016/s0896-6273(01)00485-8

Perez-Orive, J., Mazor, O., Turner, G. C., Cassenaer, S., Wilson, R. I., and Laurent, G. (2002). Oscillations and sparsening of odor representations in the mushroom body. *Science* 297, 359–365. doi:10.1126/science.1070502

Pfeiffer, B. D., Ngo, T.-T. B., Hibbard, K. L., Murphy, C., Jenett, A., Truman, J. W., et al. (2010). Refinement of tools for targeted gene expression in *Drosophila*. *Genetics* 186, 735–755. doi:10.1534/genetics.110.119917

Pitman, J. L., Huetteroth, W., Burke, C. J., Krashes, M. J., Lai, S.-L., Lee, T., et al. (2011). A pair of inhibitory neurons are required to sustain labile memory in the *Drosophila* mushroom body. *Curr. Biol.* 21, 855–861. doi:10.1016/j.cub.2011.03.069

Quiroga, R. Q., Reddy, L., Kreiman, G., Koch, C., and Fried, I. (2005). Invariant visual representation by single neurons in the human brain. *Nature* 435, 1102–1107. doi:10.1038/nature03687

Roeder, T. (2005). Tyramine and octopamine: Ruling behavior and metabolism. *Annu. Rev. Entomol.* 50, 447–477. doi:10.1146/annurev.ento.50.071803.130404

Roland, B., Deneux, T., Franks, K. M., Bathellier, B., and Fleischmann, A. (2017). Odor identity coding by distributed ensembles of neurons in the mouse olfactory cortex. *eLife* 6, e26337. doi:10.7554/eLife.26337

Saalfeld, S., Cardona, A., Hartenstein, V., and Tomancak, P. (2009). Catmaid: Collaborative annotation toolkit for massive amounts of image data. *Bioinformatics* 25, 1984–1986. doi:10.1093/bioinformatics/btp266

Sachse, S., and Galizia, C. G. (2003). The coding of odour-intensity in the honeybee antennal lobe: Local computation optimizes odour representation. *Eur. J. Neurosci.* 18, 2119–2132. doi:10.1046/j.1460-9568.2003.02931.x

Saumweber, T., Rohwedder, A., Schleyer, M., Eichler, K., Chen, Y., Aso, Y., et al. (2018). Functional architecture of reward learning in mushroom body extrinsic neurons of larval *Drosophila*. *Nat. Commun.* 9, 1104. doi:10.1038/s41467-018-03130-1

Schindelin, J., Arganda-Carreras, I., Frise, E., Kaynig, V., Longair, M., Pietzsch, T., et al. (2012). Fiji: An open-source platform for biological-image analysis. *Nat. Methods* 9, 676–682. doi:10.1038/nmeth.2019

Schneider-Mizell, C. M., Gerhard, S., Longair, M., Kazimiers, T., Li, F., Zwart, M. F., et al. (2016). Quantitative neuroanatomy for connectomics in *Drosophila*. *Elife* 5, e12059. doi:10.7554/eLife.12059

Scherer, S., Stocker, R. F., and Gerber, B. (2023). Olfactory learning in individually assayed *Drosophila* larvae. *Learning and Memory* 10, 217–255. doi:10.1101/lm.57903

Selcho, M., Millán, C., Palacios-Muñoz, A., Ruf, F., Ubillo, L., Chen, J., et al. (2017). Central and peripheral clocks are coupled by a neuropeptide pathway in Drosophila. *Nat. Comms.* 8, 15563. doi:10.1038/ncomms15563

Slater, G., Levy, P., Chan, K. L. A., and Larsen, C. (2015). A central neural pathway controlling odor tracking in *Drosophila*. *J. Neurosci.* 35, 1831–1848. doi:10.1523/JNEUROSCI.2331-14.2015

Stettler, D. D., and Axel, R. (2009). Representations of odor in the piriform cortex. *Neuron* 63, 854–864. doi:10.1016/j.neuron.2009.09.005

Stopfer, M., Jayaraman, V., and Laurent, G. (2003). Intensity versus identity coding in an olfactory system. *Neuron* 39, 991–1004. doi:10.1016/j.neuron.2003.08.011

Strother, J. A., Wu, S., Rogers, E. M., Eliason, J. L. M., Wong, A. M., Nern, A., et al. (2018). Behavioral state modulates the ON visual motion pathway of *Drosophila*. *Proc. Natl. Acad. Sci.* 115, E102–E111. doi:10.1073/pnas.1703090115

Technau, G., and Heisenberg, M. (1982). Neural reorganization during metamorphosis of the corpora pedunculata in *Drosophila melanogaster*. *Nature* 295, 405–407. doi:10.1038/295405a0

Vrontou, E., Groschner, L. N., Szydlowski, S., Brain, R., Krebbers, A., and Miesenböck, G. (2021). Response competition between neurons and antineurons in the mushroom body. *Curr. Biol.* 31, 4911–4922.e4. doi:10.1016/j.cub.2021.09.008

Wang, Y., Guo, H., Pologruto, T. A., Hannan, F., Hakker, I., Svoboda, K., et al. (2004). Stereotyped odor-evoked activity in the mushroom body of *Drosophila* revealed by green fluorescent protein-based Ca2+ imaging. *J. Neurosci.* 24, 6507–6514. doi:10.1523/JNEUROSCI.3727-03.2004

Wong, J. Y. H., Wan, B. A., Bland, T., Montagnese, M., McLachlan, A. D., O'Kane, C. J., et al. (2021). Octopaminergic neurons have multiple targets in *Drosophila* larval mushroom body calyx and can modulate behavioral odor discrimination. *Learn. Mem.* 28, 53–71. doi:10.1101/lm.052159.120

Zars, T., Wolf, R., Davis, R., and Heisenberg, M. (2000). Tissue-specific expression of a type I adenylyl cyclase rescues the rutabaga mutant memory defect: In search of the engram. *Learn. Mem.* 7, 18–31. doi:10.1101/lm.7.1.18